NASA CONTRACTOR REPORT
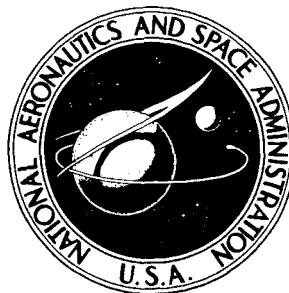
NASA CR-2449

NASA CR-2449

FLUCTUATING SURFACE-PRESSURE CHARACTERISTICS ON SLENDER CONES IN SUBSONIC, SUPERSONIC, AND HYPERSONIC MACH-NUMBER FLOW

by Hanno H. Heller and Anthony R. Clemente

Prepared by
BOLT BERANEK AND NEWMAN INC.
Cambridge, Mass. 02138
for Langley Research Center

NATIONAL AERONAUTICS AND SPACE ADMINISTRATION • WASHINGTON, D. C. • OCTOBER 1974

1. Report No. NASA CR-2449	2. Government Accession No.	3. Recipient's Catalog No.
4. Title and Subtitle FLUCTUATING SURFACE-PRESSURE CHARACTERISTICS ON SLENDER CONES IN SUBSONIC, SUPERSONIC, AND HYPERSONIC MACH-NUMBER FLOW		5. Report Date October 1974
		6. Performing Organization Code
7. Author(s) Hanno H. Heller and Anthony R. Clemente		8. Performing Organization Report No.
		10. Work Unit No.
9. Performing Organization Name and Address Bolt Beranek and Newman Inc. 50 Moulton Street Cambridge, MA 02138		11. Contract or Grant No. NAS1-9559, Task 21
12. Sponsoring Agency Name and Address National Aeronautics & Space Administration Washington, DC 20546		13. Type of Report and Period Covered Contractor Report
		14. Sponsoring Agency Code

15. Supplementary Notes

Final Report

16. Abstract

This report presents results of an experimental program to determine the flow-induced unsteady aerodynamic loads on space-shuttle orbiter configurations in the early reentry phase. Experiments on 8° half-angle cone/flat-base configurations were conducted at free-stream Mach numbers of 6 and 15 and Reynolds numbers corresponding to shuttle reentry. With these test results and pertinent results from other research efforts, data are available at free-stream Mach numbers of 0.67, 2.5, 3, 4, 6, 15, and 22. Thus, empirical expressions could be developed for the Mach-number dependence of the overall fluctuating pressure under an attached turbulent boundary layer and under a separated base-flow region.

17. Key Words (Suggested by Author(s)) Space shuttle acoustics Boundary layer noise Base pressure fluctuations	18. Distribution Statement Unclassified – Unlimited STAR Category: 23		
19. Security Classif. (of this report) Unclassified	20. Security Classif. (of this page) Unclassified	21. No. of Pages 80	22. Price* $4.00

TABLE OF CONTENTS

FLUCTUATING SURFACE-PRESSURE CHARACTERISTICS ON SLENDER CONES IN SUBSONIC, SUPERSONIC, AND HYPERSONIC MACH-NUMBER FLOW

Hanno H. Heller
Anthony R. Clemente
Bolt Beranek and Newman Inc.

SUMMARY

This report presents results of an experimental program to determine the flow-induced unsteady aerodynamic loads on space-shuttle orbiter configurations in the early reentry phase. Experiments on 8° half-angle cone/flat-base configurations were conducted at free-stream Mach numbers of 6 and 15 and Reynolds numbers corresponding to shuttle reentry conditions. The flow facilities used were the H-3 Hypersonic Facility (Mach 6) and the Longshot Free Piston Tunnel (Mach 15) of the Von Karman Institute (VKI) for Fluid Dynamics in Rhode-St-Genese, Belgium.

With these test results and pertinent results from other research efforts, data are available at free-stream Mach numbers of 0.67, 2.5, 3, 4, 6, 15, and 22. Thus, empirical expressions could be developed for the Mach-number dependence of the overall fluctuating pressure under an attached turbulent boundary layer and under a separated base-flow region.

For $0 < M < 12$, the overall fluctuating pressure $(p_{rms})_{OA}$ under an attached turbulent boundary layer normalized with the local dynamic pressure q_e has the following Mach-number dependence:

$$\frac{(P_{rms})_{overall}}{q_e} = \frac{0.006}{1 + (0.15M_e)^2 + (0.15M_e)^4} , \qquad (S-1)$$

where M_e is the edge Mach number. Equation S-1 is shown in Fig. 42 with supporting experimental data.

The average overall normalized fluctuating pressure on the flat base of a slender cone was found to have the following Mach-number dependence:

$$\frac{(p_{rms})_{OA}}{q_\infty} = \frac{1}{56 \cdot |M_\infty^2 - 1|} \quad , \tag{S-2}$$

where q_∞ and M_∞ represent the free-stream conditions. Equation S-2 is shown in Fig. 45 with supporting experimental data. This equation is believed to be valid for $0 < M < 22$, except for $M_\infty = 1$ where the function blows up.

Furthermore, experimental data allowed the definition of a nondimensional base-pressure spectrum for a Mach-number range comprising at least $0.67 < M_\infty < 6$. This spectrum is shown in Fig. 25.

INTRODUCTION

Definition of the unsteady aerodynamic load characteristics during the entire flight trajectory of a spacecraft is an essential part of the structural design phase, as well as of the flight-planning phase. The United States Space Shuttle features a manned reusable delta-winged orbiter on top of a combination of liquid and solid propellant booster rockets to lift payload in earth orbit. This configuration differs from the "Apollo" configuration, because the flight bodies are not rotationally symmetrical. Therefore, in the ascend and reentry phases, the flight bodies are exposed to loads which should differ characteristically from those experienced by the Apollo launch configuration or the command capsule, respectively.

Some studies (see, for example, Coe *et al*, 1971) were conducted to obtain information on the fluctuating-pressure characteristics on the surface structure of shuttle models at Mach numbers corresponding to the subsonic and low supersonic flight regime. Recently, Bolt Beranek and Newman Inc. (BBN) under contract with the NASA-Langley Research Center measured pressure spectra on a cone/flat-base configuration and on a straight-wing orbiter model in the Mach-number range of 0.67 to 4.0 (Heller and Holmes, 1971).

Now that the final shuttle configuration is defined, it is desirable to determine the flow-induced unsteady aerodynamic load characteristics over the entire reentry phase. This study includes the hypersonic Mach-number range where rapid heating makes conditions critical. The primary objective of the study is the experimental characterization of surface pressure fluctuations at high hypersonic ($M>8$) Mach numbers, where reliable information presently is unavailable.

To conduct appropriate model tests, a flow facility, which closely simulates the important parameters of a typical reentry flight, is needed. The only facility that provides Reynolds-number similarity at hypersonic Mach numbers (15<M<24) is the "Longshot Free Piston Hypersonic Tunnel" of the Von Karman Institute (VKI) for Fluid Dynamics at Rhode-St-Genese in Belgium. This shock-tunnel facility provides flow for a few milliseconds. Another facility at the VKI, the Hypersonic Tunnel H-3, provides continuous high Reynolds-number flow at a Mach number of 6. (These facilities are described in more detail in Appendix A.)

Before tests on complicated configurations, i.e., orbiter configurations, could be attempted, a series of experiments on simple bodies (8° half-angle cones with flat bases) were necessary to develop the required experimental techniques. Specifically, the technology had to be developed to obtain fluctuating-pressure data within the extremely short time span that undisturbed flow conditions can be established over a model in the test section of a shock tunnel. For this purpose, fast-response microphones were developed; these combined small size, high pressure and low vibration sensitivity with sufficient structural strength to withstand the test environment. Because of the short signal duration, some ingenuity was required to (1) locate the signal on tape; (2) determine the period during which the signal corresponds to an undisturbed flow situation; (3) Fourier-analyze this signal window in a frequency range up to 320 kHz; and (4) interpret the results and relate them to those results obtained on similar bodies at lower and higher Mach numbers.

TECHNICAL DISCUSSION

Reentry Environment

Simulation of the flow environment around a scaled test body in a wind tunnel requires essentially Mach number, Reynolds number, dynamic pressure, and temperature simulation.

North American Rockwell provided BBN with the latest (December 1972) reentry profile estimates. Dynamic pressure, Mach number, and unit Reynolds number are shown as function of reentry elapsed time in Fig. 1. Two points (in time after reentry) were selected for testing:

Time	1100 sec	1600 sec
M_∞	15	6
Re/ft	$\approx 4.5 \times 10^4$	14.5×10^4
q_∞	100 psf	150 psf

If the conical bodies were considered to represent 1:100 scaled models of the orbiter configuration, then unit Reynolds numbers of 4.5×10^6 and 14.5×10^6 per ft for Mach numbers of 15 and 6, respectively, are required in the flow facilities.

Simulation in Flow Facilities

The *VKI Hypersonic Tunnel H-3* (Fig. 2) is an intermittent facility of the blow-down type giving a uniform free jet 12 cm (5 in.) in diameter. A supersonic ejector provides suction downstream of the diffuser. Stagnation pressure ranges from 100 to 500 psi with stagnation temperatures up to 725° K (840° F). Free-stream Mach number is 6, unit Reynolds numbers up to 16×10^6 per m ($\approx 5 \times 10^6$ per ft) can be achieved.
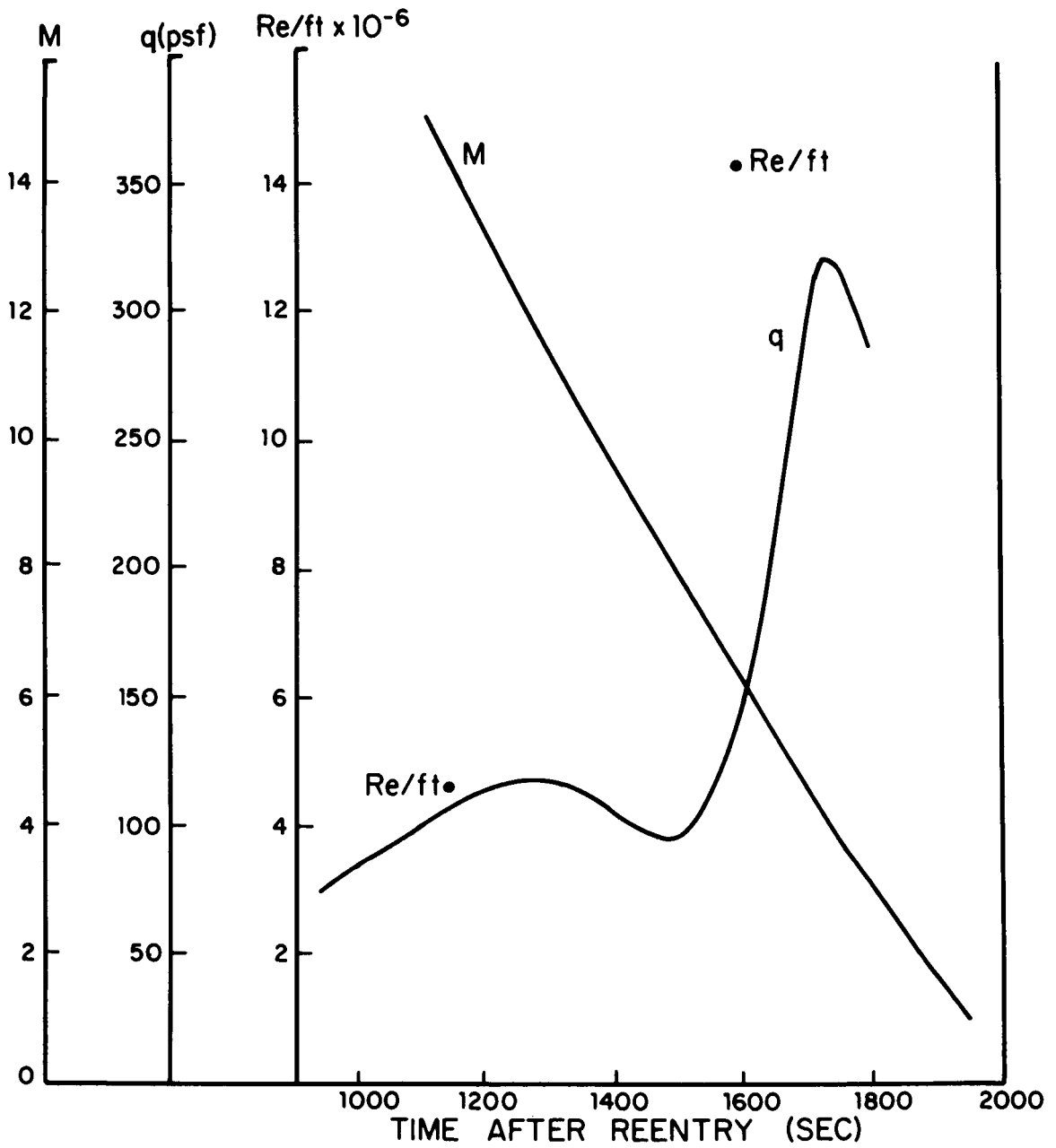
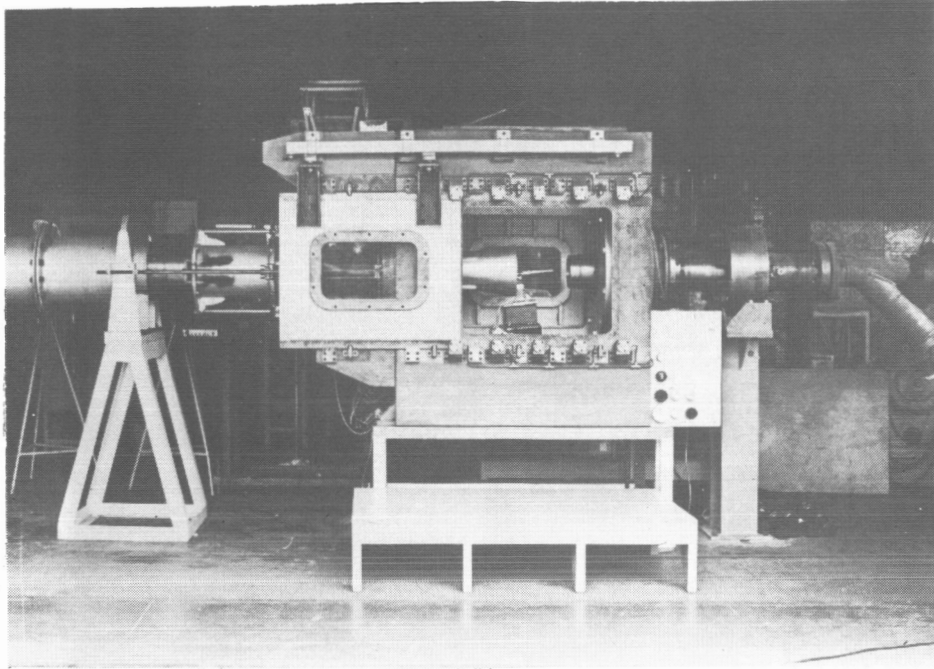FIG. 1.   REENTRY PARAMETERS FOR SPACE SHUTTLE ORBITER

FIG. 2. THE VON KARMAN INSTITUTE HYPERSONIC TUNNEL, H-3

The *VKI Longshot Free-Piston Tunnel* (Fig. 3) is an inter-
mittent facility operating with nitrogen. Its conical nozzle
diameter is 36 cm (14 in.); free-stream Mach numbers range from
15 to 24. Stagnation pressures up to 60,000 psi, with maximum
stagnation temperature of 2600° K, are attainable. Unit Reynolds
numbers range from 10 to 33×10^6 per m (3 to 10×10^6 per ft).

Thus, the H-3 facility is capable of providing Reynolds num-
ber that are close to those required. The Longshot facility
provides a range of Reynolds number well within those required.

Experimental
Models

In both the H-3 and the Longshot (LS) tests, 8° half-angle/
flat-base cones are used. They are supported with wedge-shaped
pylons, through which instrumentation leads are fed. In the H-3
tests, the cone was 26.5 cm (10.5 in.) long, with a base diameter
of 7.5 cm (3 in.); the cone model is shown in the test section
of the H-3 tunnel in Fig. 4. In LS, the cone length was 53.5 cm
(21 in.) with a base diameter of 15 cm (6 in.); this cone is
shown in the LS tests chamber in Fig. 5.

Model Instrumentation

Both models were equipped with (1) fluctuating-pressure sen-
sors, (2) accelerometers, and (3) heat-transfer sensors. All
instrumentation was developed and fabricated by BBN.
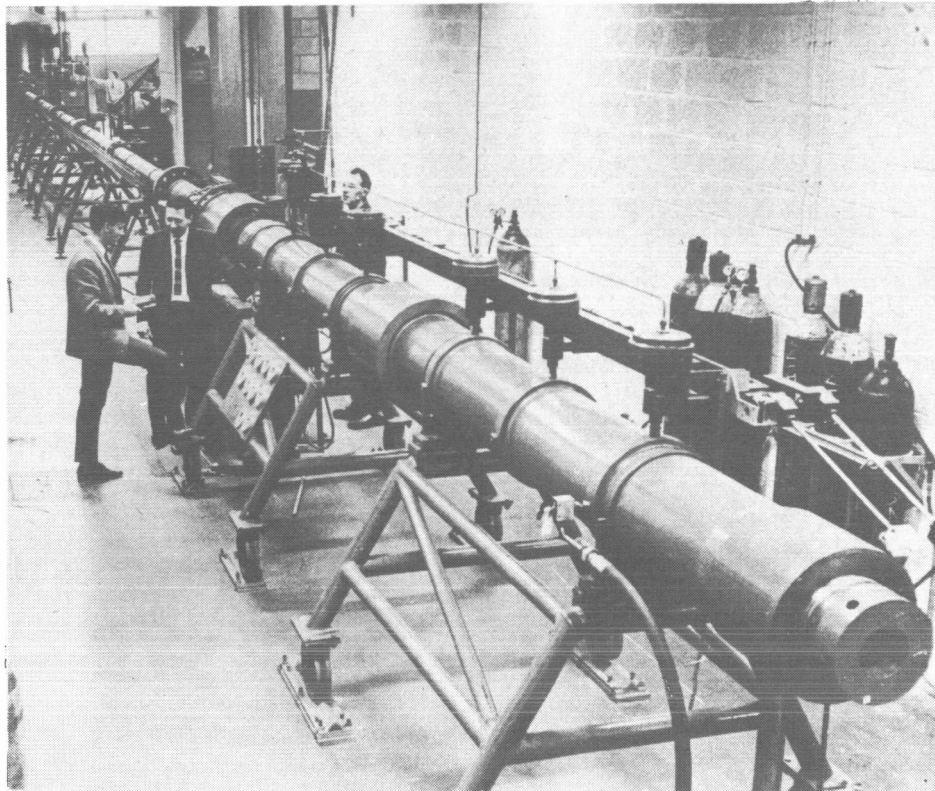
8

FIG. 3.   THE VON KARMAN INSTITUTE "LONGSHOT" TUNNEL
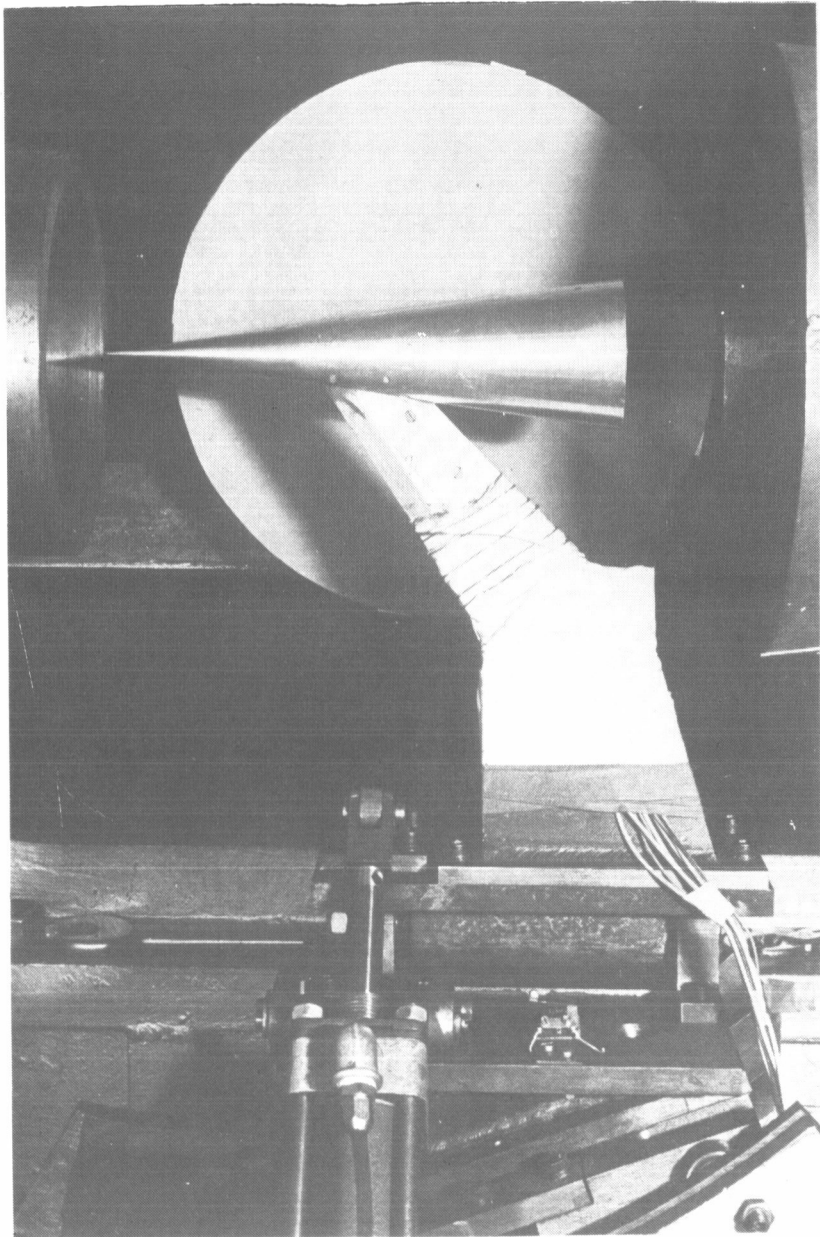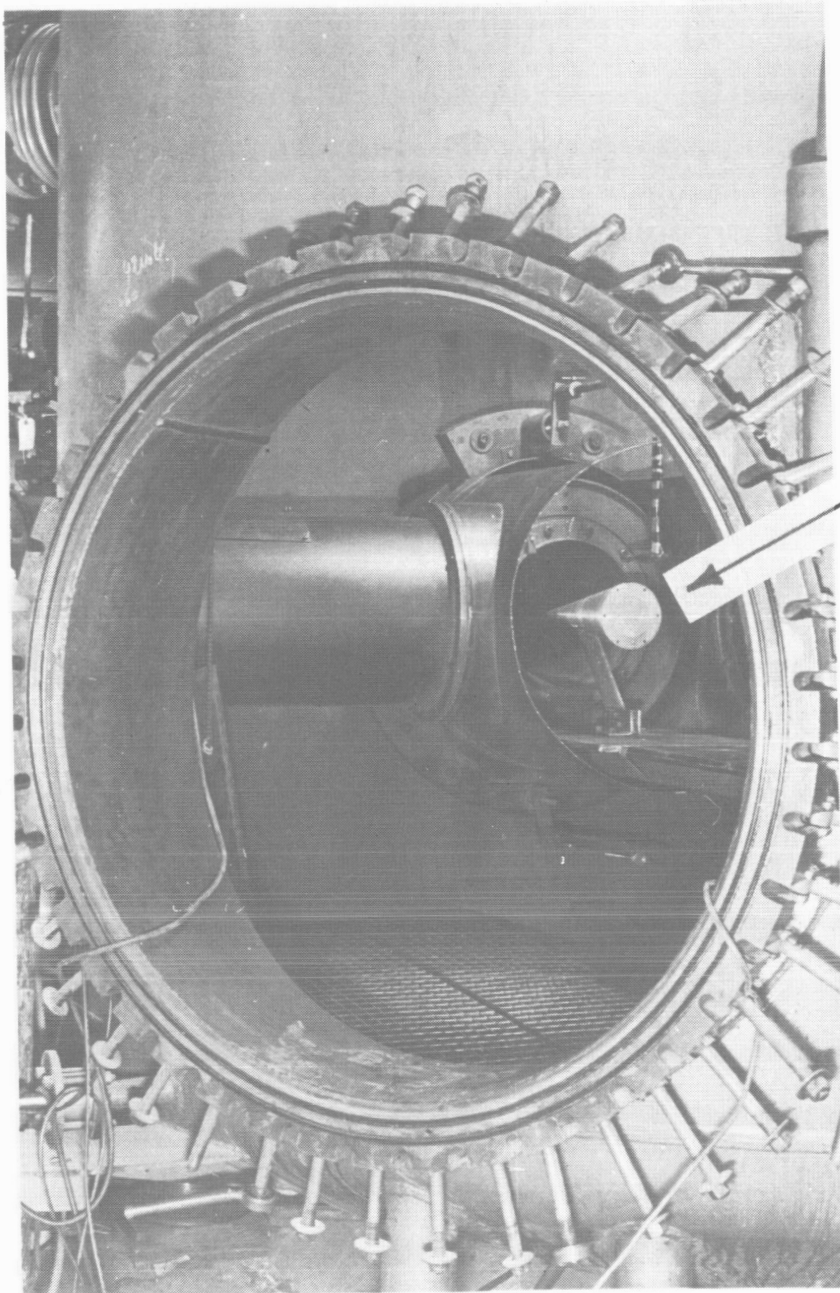
FIG. 4.   8° HALF-ANGLE CONE/FLAT-BASE CONFIGURATION IN TEST
           SECTION OF H-3 FACILITY (CONE LENGTH: 26.5 cm)

Model

FIG. 5.   VIEW INTO TEST CHAMBER OF THE LONGSHOT FACILITY AT
          VKI WITH 8° HALF-ANGLE CONE/FLAT-BASE CONFIGURATION
          (CONE LENGTH: 53.5 cm)

Pressure Sensors

Because of the extremely thin turbulent boundary layer ex-
pected on the cone surface, the effective sensing diameter of
the microphones must be as small as possible while still providing
sufficient sensitivity for the expected signal. BBN 1/10-in.
diameter piezoelectric pressure sensors (type 377) with internal
impedance matching circuit were used. These sensors (including
FET circuit) are 0.28 cm (0.11 in.) diameter by 1.9 cm (0.75 in.)
long; sensing diameter is 0.20 cm (0.08 in.). Sensitivity is
about -115 dB re 1 V/μbar over a frequency range from 50 Hz to
beyond 200,000 Hz; resonance frequency is above 250,000 Hz.
These sensors were mounted flush to the cone surface. Similar
sensors (BBN type 376) with a sensing-area of 0.56 cm (0.22 in.)
diameter, and outside dimensions of 0.635 cm (0.25 in.) diameter
by 2.54 cm (1 in.) long were used on the base of the models.
Their sensitivity is about -103 dB re 1 V/μbar, over a frequency
range from 50 Hz to 20,000 Hz. Resonance occurs at about 50,000
Hz. The installed sensors were covered with an RTV layer,
smoothed to the surface contours. This technique, which has been
used in the past, shows no evidence of deterioration in sensor
performance. Flow tests were conducted to assure that the sensor
presence did not prematurely trigger a laminar boundary layer.

Accelerometers

BBN type 501 accelerometers (with internal impedance match-
ing FET circuit) are mounted inside the models with their axes
parallel to the axes of the sensors. Thus, the portion of the
signal that must be attributed to vibration can be assessed.

Heat Transfer Gauges

BBN type T/C 100 gauges are located on the cone surface to provide information on the state of the cone-surface boundary layer (laminar vs turbulent). These gauges supplement the information obtained through schlierenoptical and shadowgraph-type flow visualization.

Data Acquisition System

The signals from the pressure and vibration sensors (both contain the internal preamplifier, which lowers the output impedance to about 1200Ω) were fed through amplifiers with an adjustable gain from 0 to 66 dB and a flat frequency response from 2 Hz to beyond 1 MHz into a Honeywell Model 5600 Portable Tape Recorder.

In all tests, data were recorded at 60-ips tape speed. The recorder operates in the AM (direct record) and in the FM mode. Recordings in the AM mode at 60 ips provide a response range of 300 Hz to 300,000 Hz. Consequently, the signals of all the forward cone sensors with a frequency response in excess of 200,000 Hz and the accelerometers with a flat response up to 50,000 Hz were recorded on the AM channels. In the "doubly extended mode", the FM channels provide a response range from dc to 40,000 Hz; signals from the base sensors with a frequency response in excess of 20,000 Hz were recorded on the FM channels. Some signals were also monitored on oscilloscopes for a "quick-look inspection" of data during (H-3) or after (LS) the test runs. Polaroid photographs were also taken.

Data Reduction

The H-3 data obtained at a Mach number of 6 are of interest *per se*. They fall in a Mach-number range where only limited data on fluctuating surface pressures are available. However, the primary purpose of the H-3 tests was to check out the data acquisition and reduction procedures to be used in the LS tests under controlled and well-known conditions; H-3 provided flow for time periods of several tens of seconds, while a typical LS shot lasts for only 20 msec. For this reason, H-3 data was not reduced by feeding taped signals into a conventional spectrum analyzer; instead, the following procedure was adopted:

Signals on the AM channels were slowed down through repeated re-recordings in the following manner:

Recording at 60 ips to provide bandwidth   400 Hz — 300 kHz

Playback at 7-1/2 ips to provide bandwidth   50 Hz — 37.5 kHz

Transfer to second tape recorder
  recording at 120 ips in FM extended
mode to provide bandwidth   50 Hz — 40 kHz

Playback at 3-3/4 ips to provide bandwidth 1.56 Hz — 1.25 kHz

Signals on the FM channels were slowed down as follows:

Recording at 60 ips to provide bandwidth   0 Hz — 40 kHz

Recording in FM double-extended mode
  playback at 1-7/8 ips to provide
bandwidth   0 Hz — 1.25 kHz

In each case, the resulting continuous signals have a frequency content up to 1.25 kHz.

Thus, the AM signals undergo a "downward" frequency scaling by a factor of 256, the FM signals by a factor of 32. Before feeding the (slowed-down) signals into the Adage analog-to-digital converter, the signals from the Honeywell recorder were amplified by a factor of 100, to have the full 14-bit range of the Adage available. After the A- to D-conversion, a Fourier analysis was performed on a DEC-PDP-15-35 digital computer with a 16-K memory.

The Fourier analysis uses discrete signals, which are given as a succession of N signal values x_j.

The so-called Discrete Fourier Transform is:

$$S_k = \frac{1}{\sqrt{N}} \sum_{j=0}^{N-1} x_j \, e^{-2\pi i \cdot jk/N} \quad \text{with} \quad k = 0,1,2 \cdots\cdots, N-1 \quad .$$

If the discrete values x_j are samples taken at intervals Δt from a continuous signal $f(t)$, then: $x_j = f(j \cdot \Delta t)$.

It might be expected that the Fourier transform of the series x_j would be equal to samples taken from the Fourier transform applied to the continuous signal $f(t)$. Such a correspondence exists only when the signal $f(t)$ has a Fourier transform that is zero outside the frequency-range $1/2\Delta t$. The so-called aliasing-effect error is avoided by transmitting the AM and FM signals through a low-pass filter with cutoff frequency at 1.25 kHz. As mentioned earlier, real-time analysis up to 320,000 Hz (of the cone-surface flow data) is desired. Slowing the tape signal down by a factor of 256 makes this frequency correspond to 1250 Hz. This frequency now becomes the highest frequency of interest.
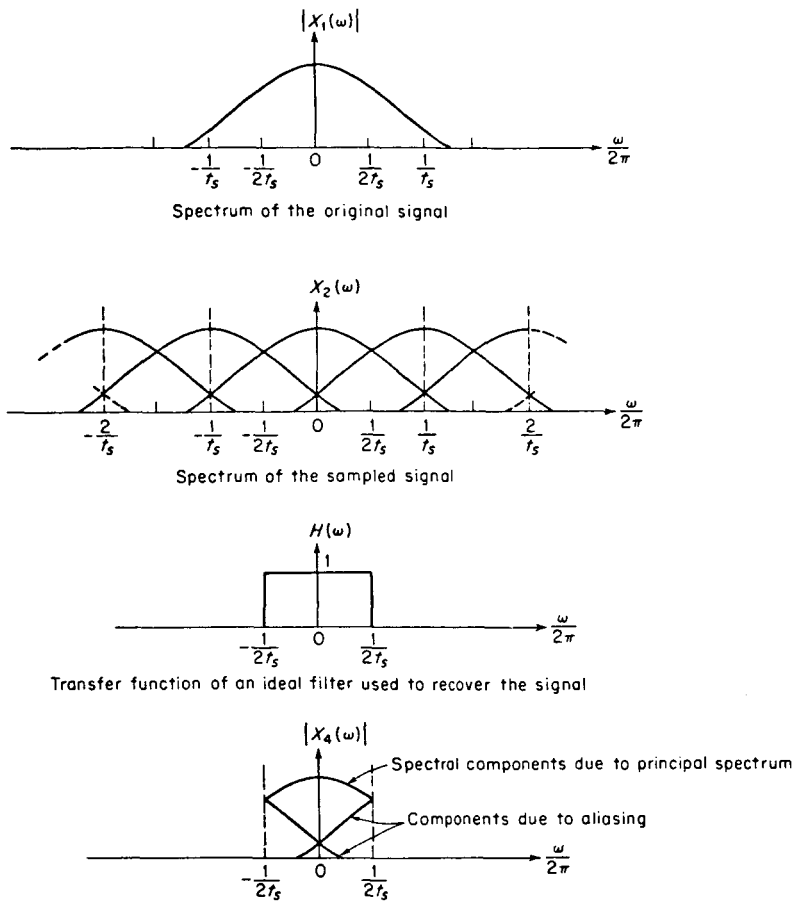
However, there will be spectral components higher than 1250 Hz. So that these components will not affect the sampling of the

original spectrum, the sampled spectrum at 1250 Hz must be (1) cut-off (by means of a low-pass filter) and (2) this frequency must be half the sampling frequency. The need for this halving becomes apparent from Fig. 6, which explains the aliasing effect. Thus, the sampling frequency becomes 2 × 1250 Hz = 2500 Hz. In turn, the sampling frequency then fixes the sampling window, which is the reciprocal of 2500 Hz, i.e., 400 μsec long. Since the 16-K memory of the computer allows a maximum of 1000 core samples, we can analyze a total time span of 1000 times 400 μsec or 0.4 sec. In turn, this corresponds to 0.4/256, i.e., 1.6 msec in real time.

Thus, the problem becomes one of selecting from the available short-duration signals of the LS test series an appropriate 1.6 msec signal window for analysis up to 320,000 Hz. The selection of these windows will be discussed later in the context of the LS tests. For analysis up to 320,000 Hz of the H-3 data, an arbitrary 1.6 msec sample from the total available test time was selected and processed as described.

Base-pressure data obtained with the 1/4-in. diameter type 376 BBN sensors required analysis only up to 40 kHz. Consequently, tape signals needed to be slowed down only by a factor of 32, to make the highest frequency analyzed in the DEC-PDP-15-35 equal to 1250 Hz. Thus, for FM-channel data reduction, the sampling frequency becomes 6667 Hz, with a corresponding (real time) window width of 4.8 msec.

The software program provides a print-out of the sampled data, a copy into mass storage (disk or DEC tape), and a graphic display.

$|X_1(\omega)|$

Spectrum of the original signal

$X_2(\omega)$

Spectrum of the sampled signal

$H(\omega)$

Transfer function of an ideal filter used to recover the signal

$|X_4(\omega)|$

Spectral components due to principal spectrum

Components due to aliasing

Example of aliasing. The original spectrum $X_1(\omega)$ is broader than half the sampling frequency $1/t_s$. Thus, the spectrum of the sampled signal, $X_2(\omega)$ is composed of overlapping spectra. When filtered, the original spectrum within the filter band is not recovered, but contains also components due to aliasing.

FIG. 6. THE ALIASING EFFECT (Reproduced from L.L. Beranek, 1971, *Noise and Vibration Control*, New York, N.Y.)

The sampling is started from a pulse produced by a variable counter, which is activated by a triggering signal on one of the tape channels.

Once in memory and arranged in an array, the data are shuffled so that their indexes, when written as binary numbers, appear left-right inverted. The Fast Fourier Transform is further implemented by multiplying the data with an appropriate complex exponential value and restoring the results in the same memory locations as the original data values. This procedure is repeated several times for all N data, generating the Fourier coefficients in the array itself. These coefficients may be printed or plotted on a log-log diagram, resulting in the final graphs (see Fig. 7).

The plot in Fig. 7 represents the analyzed signal of a rear cone sensor in terms of a signal output 20 log V/V_0 (where V_0 is an arbitrary reference voltage) vs a logarithmic frequency. Since the analysis pertains to a plotted frequency range of 2.5 Hz to 1250 Hz, each data point represents the energy in a constant *absolute* frequency band of 1250 Hz/512, i.e., a 2.5 Hz band. Converting this spectrum into a per-Hz spectrum lowers the levels by 4 dB. To convert this spectrum into a 1/3-octave band spectrum (with constant *relative* bandwidth), (10 log f - 6.75) dB is added to the per-Hz spectrum, where f is the 1/3-octave band center frequency. Hence, to convert the original spectra into a 1/3-octave band spectra, (10 log f - 10.75) dB must be added. Figure 7 also shows this correction curve.

Systems Calibration

The sensitivity of the pressure sensors, accelerometers, and heat flux gauges was determined prior to their installation
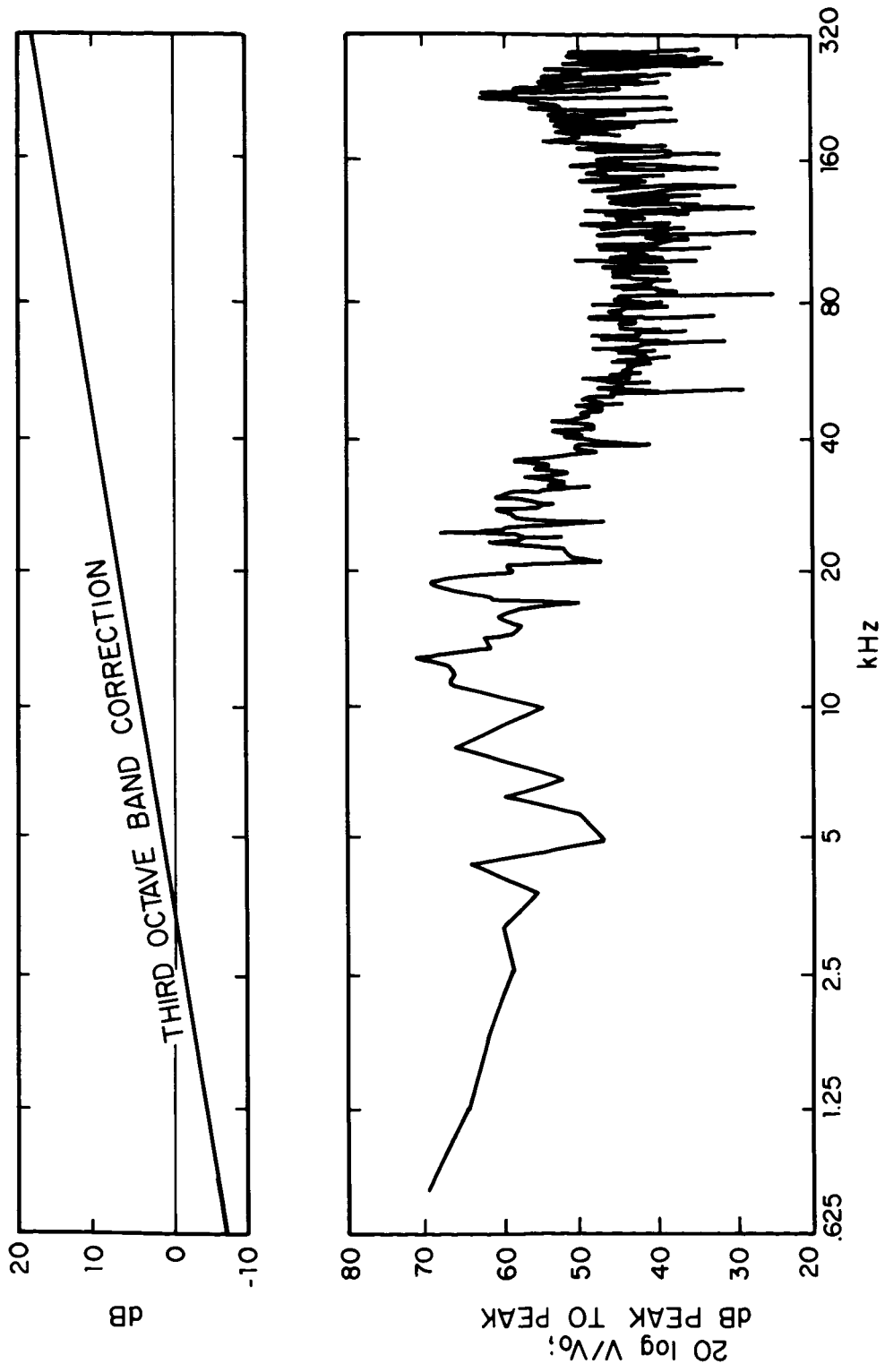
FIG. 7. SAMPLE OF DATA PRINT AND CORRECTION TO CONVERT PRINT-OUT SPECTRUM INTO 1/3-OCTAVE BAND SPECTRUM

19

in the models. Thus, in order to relate sensor voltage to the
logarithmic voltage ratio (plotted as the ordinate of the spectrum
in Fig. 7), the entire system encompassing the preamplifier, tape
recorders, A-to-D converter, and computer was calibrated by
"replacing the sensor" with an input signal of similar strength.
This signal strength was fairly low, about 10 mV; discrete signals
at frequencies 2.5, 25, and 250 kHz, of 10 mV peak to peak, were
fed into each of the channels. Figure 8 shows a typical calibra-
tion result for a 10 mV signal at 250 kHz. This signal results
in a "plotter level" of 75.5 dB re arbitrary voltage. Figure 9
shows the "plotter levels" as a function of the amplifier gain
(the only quantity that was variable in the measurement system)
for different input voltages. Thus, from a given plotter level
and the known amplifier gain, the input voltage into the system
(which is the output signal of the sensor) can be deduced. Using
Figure 10, this signal can be related to peak-to-peak fluctuating
pressure level re 2×10^{-4} μbar for any sensor sensitivity.

Test Results

Mach-6 tests

Sensor Location

Figure 11 presents a closeup view of the model retracted
from the test section of the H-3 facility. It shows the heat-
transfer sensors, the 1/10-in. pressure sensors (two near the
apex, two near the rear of the cone), and the 1/4-in. pressure
sensors on the base. Figure 12 gives the locations of the sensors.
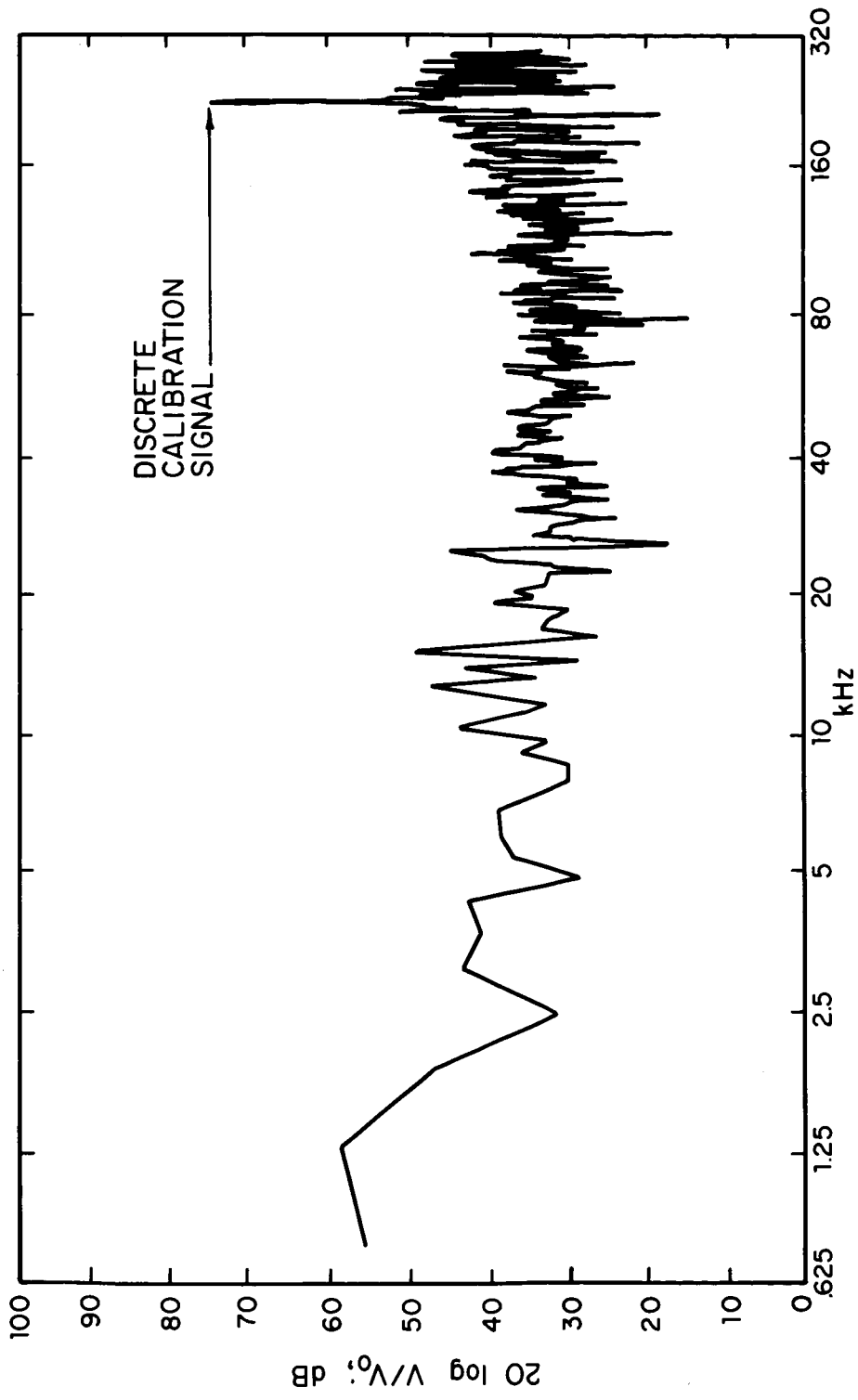
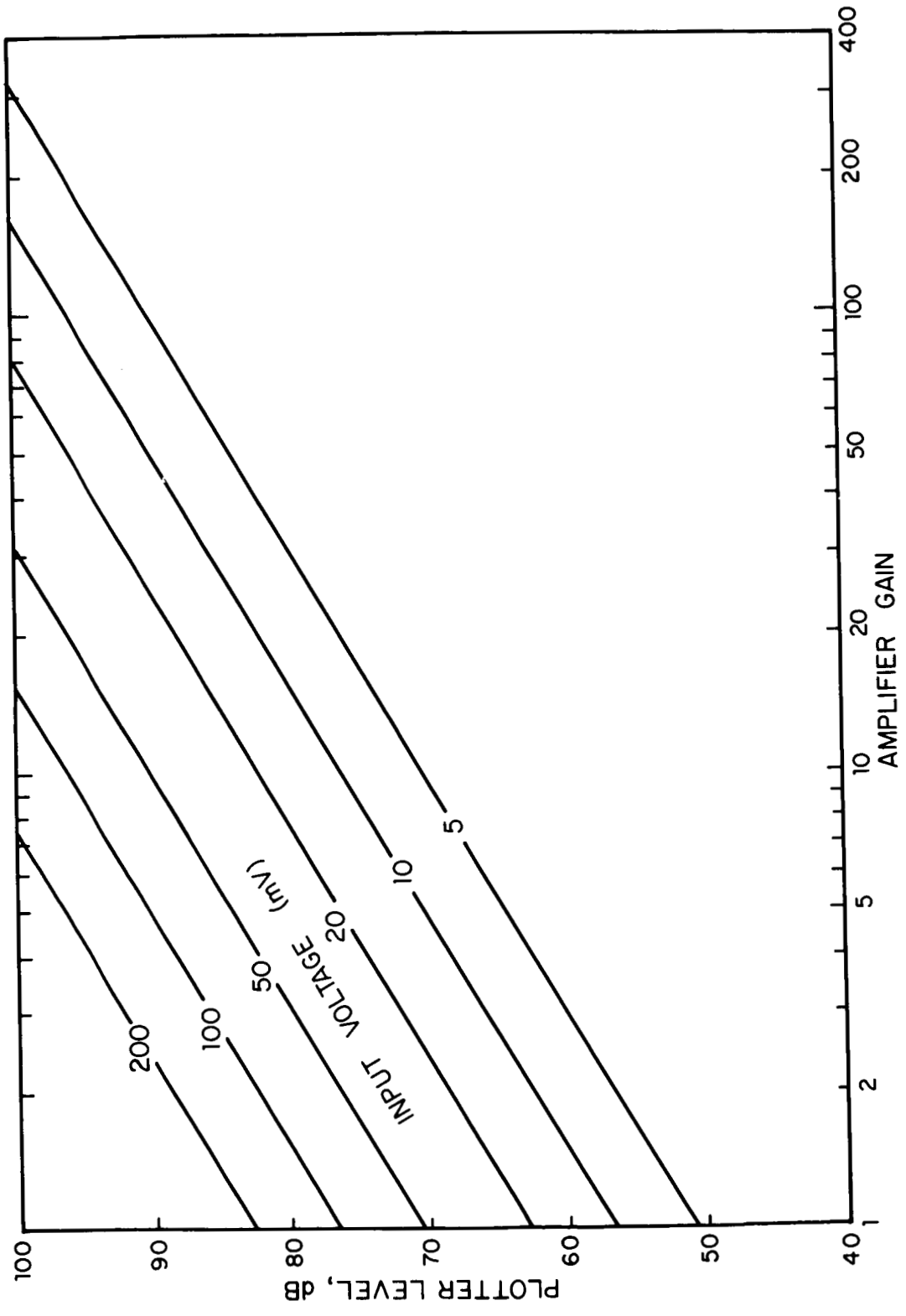FIG. 8.   TYPICAL CALIBRATION PLOT: INPUT SIGNAL OF 10 mV PEAK-TO-PEAK
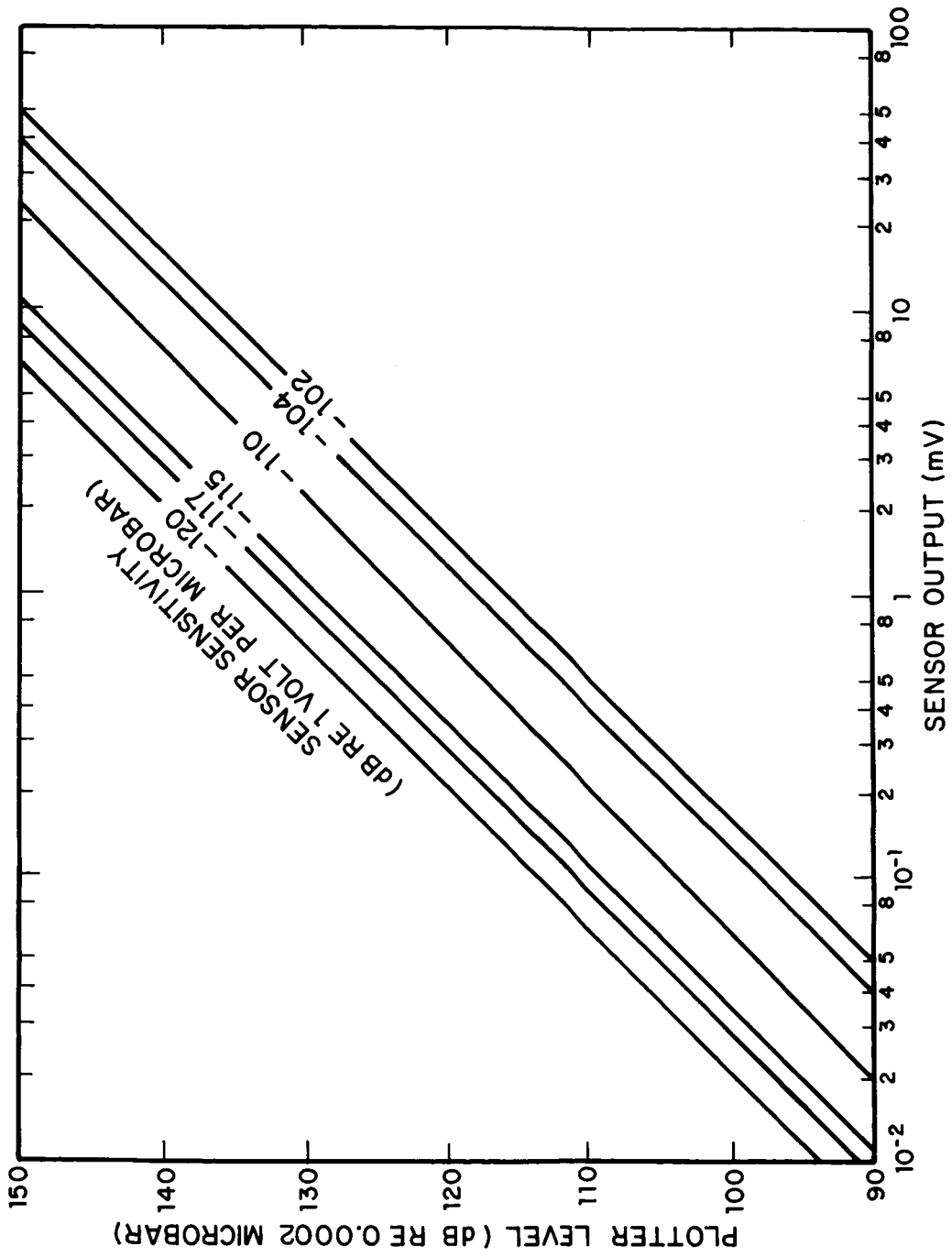
AT 250 kHz

FIG. 9. SYSTEMS CALIBRATION

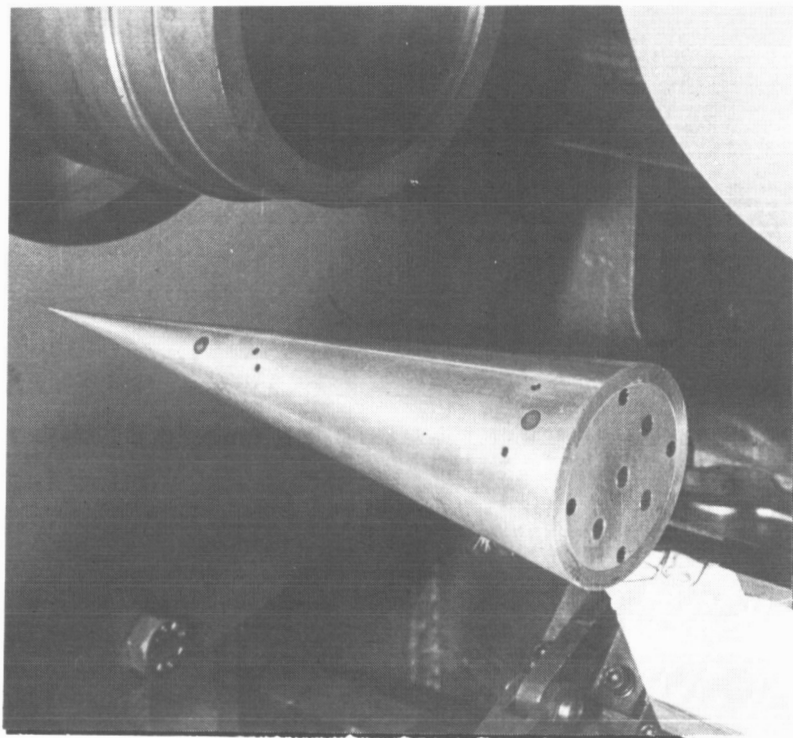22

FIG. 10. SENSOR CALIBRATION
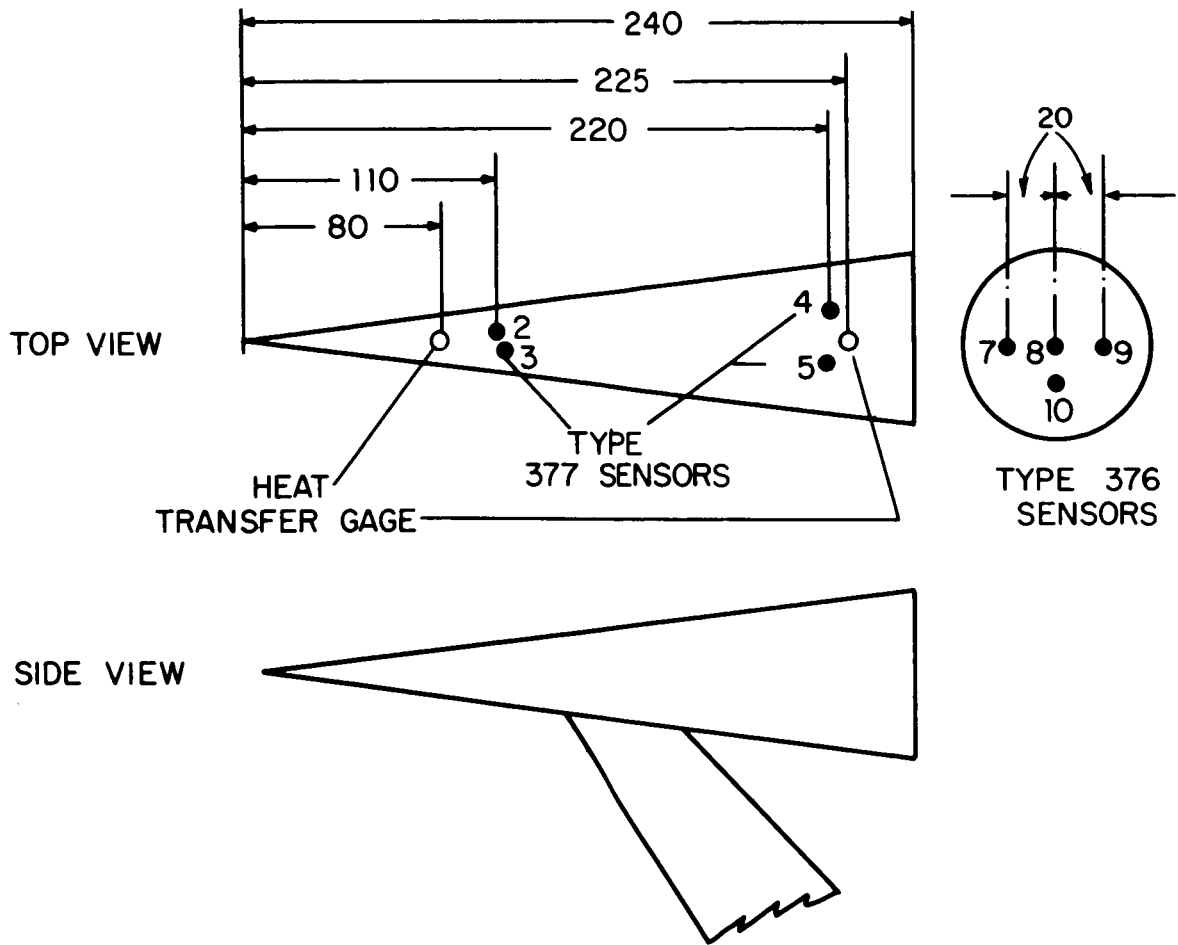
FIG. 11.   CLOSEUP VIEW OF MODEL IN H-3 FACILITY

FIG. 12. SENSOR LOCATIONS ON MODEL IN H-3 FACILITY
(Dimensions in mm)

Flow Conditions

Free-stream data are computed from data obtained through temperature and (steady-state) pressure sensors located in the plenum chamber upstream of the nozzle threat. Data are obtained for two stagnation pressures. The corresponding flow parameters are as follows:

Stagnation Pressure P_0 in atm (psia)	30	(455)	10	(159)
Stagnation Temperature T_0 in °K (°F)	453	(761)	445	(748)
Free-Stream Mach number M_∞	6		6	
Free-Stream Flow Speed U_∞ in m/sec (ft/sec)	894	(2935)	884	(2900)
Free-Stream Dynamic Pressure q_∞ in atm (psia)	0.49	(7.2)	0.17	(2.5)
Free-Stream Unit Reynolds number per m (per ft) times 10^{-6}	16	(4.95)	5.8	(1.75)
Cone-Surface Mach number	5.3		5.3	
Cone-Surface Dynamic Pressure in atm (psia)	0.82	(12.1)	0.27	(4)
Cone-Unit Reynolds number per m (per ft) times 10^{-6}	25.5	(7.75)	8.9	(2.7)

Thus, Reynolds numbers (based on the distance from the cone tip to the sensors) at the cone sensors were:

P_0 atm	30	10	
$Re \times 10^{-6}$	2.8	1.0	forward sensors
	5.6	1.95	rear sensors

A plot of transition Reynolds number vs Mach number (Fig. 13) indicates that the rear sensors were under a transitional or fully developed turbulent boundary layer for the high-Re case; in the low-Re case, both the rear cone and the apex sensors were under laminar flow.

Flow Visualization

Schlieren optical visualization of the flow around an identically shaped body supports the above statement of having turbulent flow near the cone base for the high-Re case, and laminar flow over the entire cone surface for the low-Re case (Figs. 14 and 15).

Boundary-layer dimensions were estimated from the schlieren photographs as well as from empirical schemes. For the high-Re case, schlieren photos suggest a boundary layer thickness near the base of 0.20 cm (0.085 in.). Turbulent boundary-layer thickness was measured on an $8°$ half-angle cone in the previous effort (Heller and Holmes, 1971) in the MIT wind tunnel* at lower Mach numbers and lower stagnation pressures. This information can be used to extrapolate towards the flow conditions on the cone tested in the VKI H-3 facility at Mach 6, via the following relationship:

$$\frac{\delta_{VKI}}{\delta_{MIT}} = \frac{L_{VKI}}{L_{MIT}} \cdot \left(\frac{Re_{MIT}}{RE_{VKI}}\right)^{1/5} \quad ,$$

where δ is the boundary-layer thickness, and Re is the Reynolds number based on the distance L from the visually determined transition point to the sensor location. This procedure results

———————

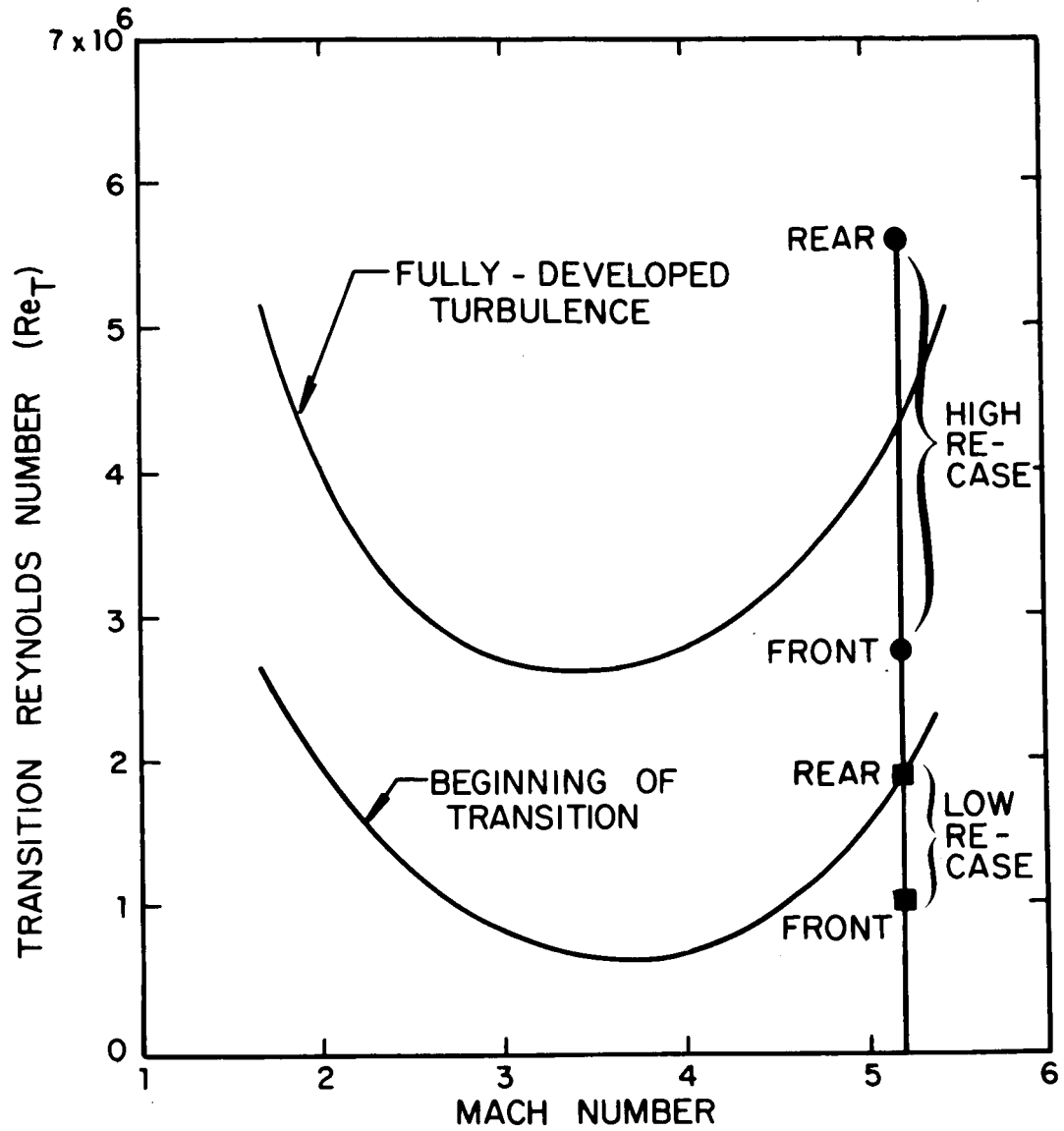*Massachusetts Institute of Technology NAVAL Supersonic Wind Tunnel.

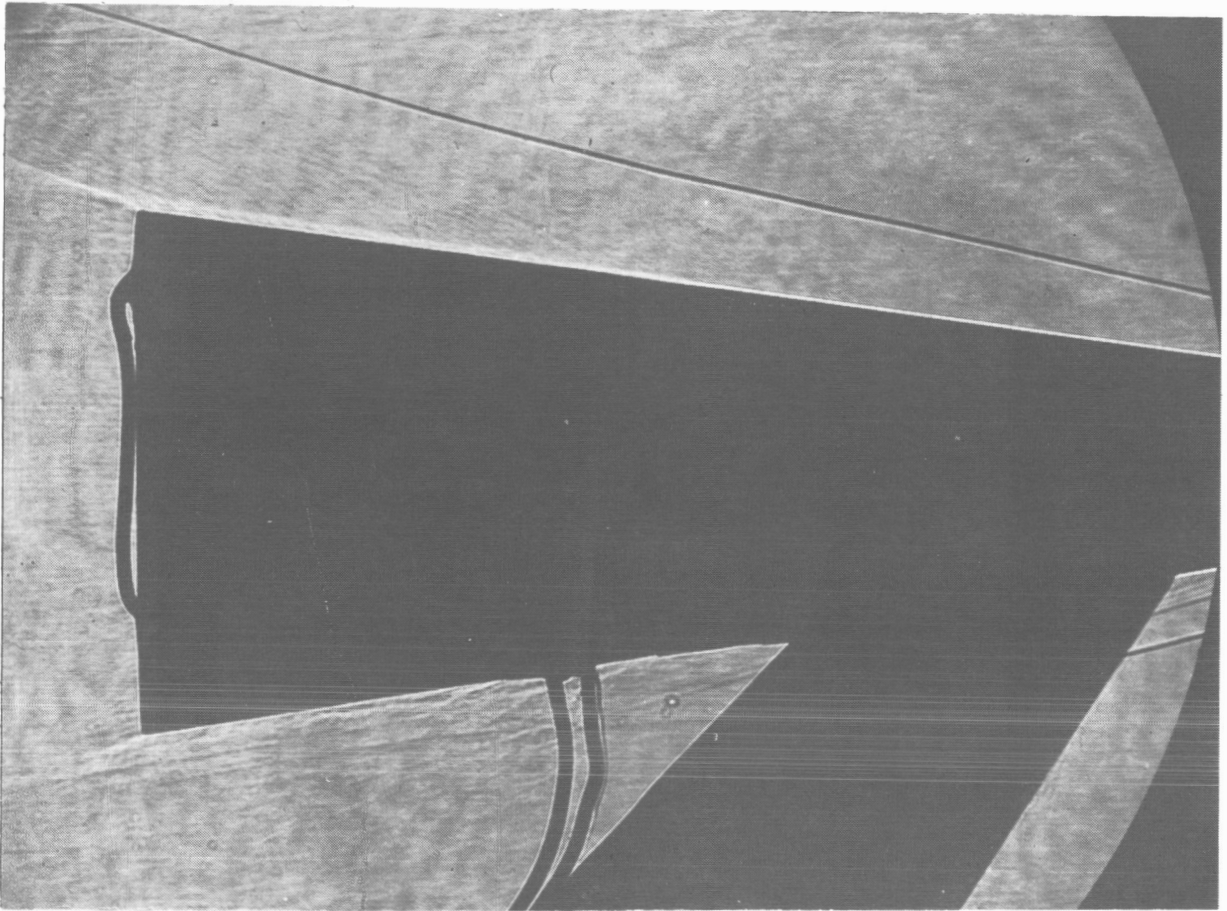FIG. 13. TRANSITION REYNOLDS NUMBER AS FUNCTION OF MACH NUMBER

FIG. 14. HIGH REYNOLDS-NUMBER FLOW OVER CONE SURFACE →
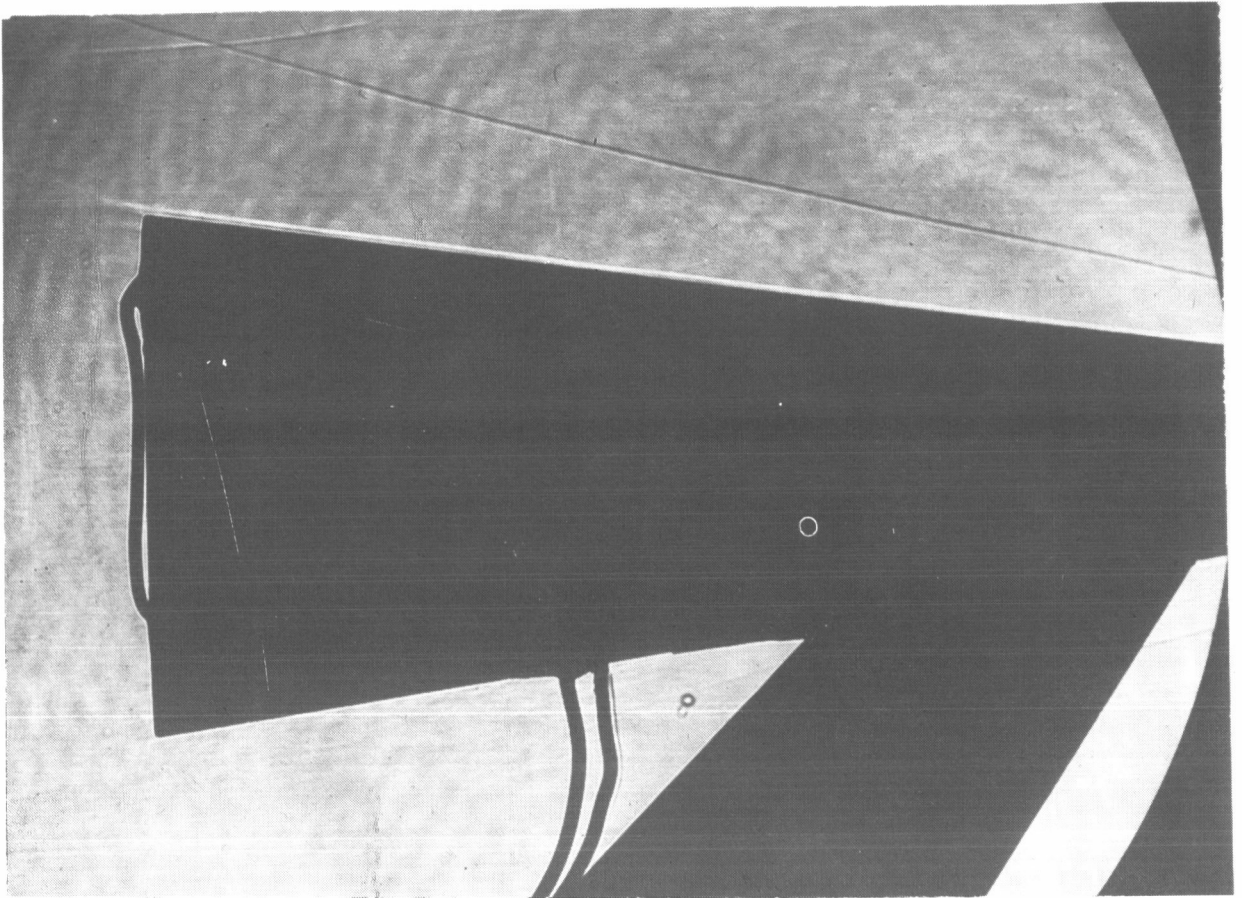TURBULENT BOUNDARY LAYER

FIG. 15. LOW REYNOLDS-NUMBER FLOW OVER CONE SURFACE →
          LAMINAR BOUNDARY LAYER

in an estimated boundary-layer thickness at the rear cone
sensors of 0.19 cm (0.075 in.), which is close to the visually
determined value.

Heat Transfer Data

The heat transfer measurements for the high Reynolds number
case yielded an average value of the heat transfer rate
$\dot{q} = 1.55$ ($\pm$ 0.17) $\times$ 10^6 [ergs/(cm^2)(sec)] {0.137 $\pm$ 0.015
[BTU/(ft^2·sec)]} at the forward sensor location, and of
$\dot{q} = 6.08$ ($\pm$ 0.22) $\times$ 10^6 [ergs/(cm^2)(sec)] {0.535 $\pm$ 0.020
[BTU/(ft^2·sec)]} at the rear-cone sensor locations.

Thus, the heat transfer rate at the rear cone sensor is about
four times higher than at the forward sensors, indicating a tur-
bulent flow state at the rear-cone sensor location.

Fluctuating-Pressure Measurements

Fourteen tests were conducted with the cone model at various
locations within the flow to identify the effects of localized
acoustic fields on the signals.

1. Forward cone data. Figure 16 shows fluctuating-pressure
level (FPL) spectra obtained from sensor No. 3 (forward cone) in
a frequency range from 625 Hz to 320,000 Hz. The scatter between
different runs is substantial up to about 20,000 Hz; this is so
basically because the data processing and analysis provide only
a few points at these relatively low frequencies. Above 20 kHz,
the data point density permits fairly accurate data averaging.
The effect of locating the model at different places in the test
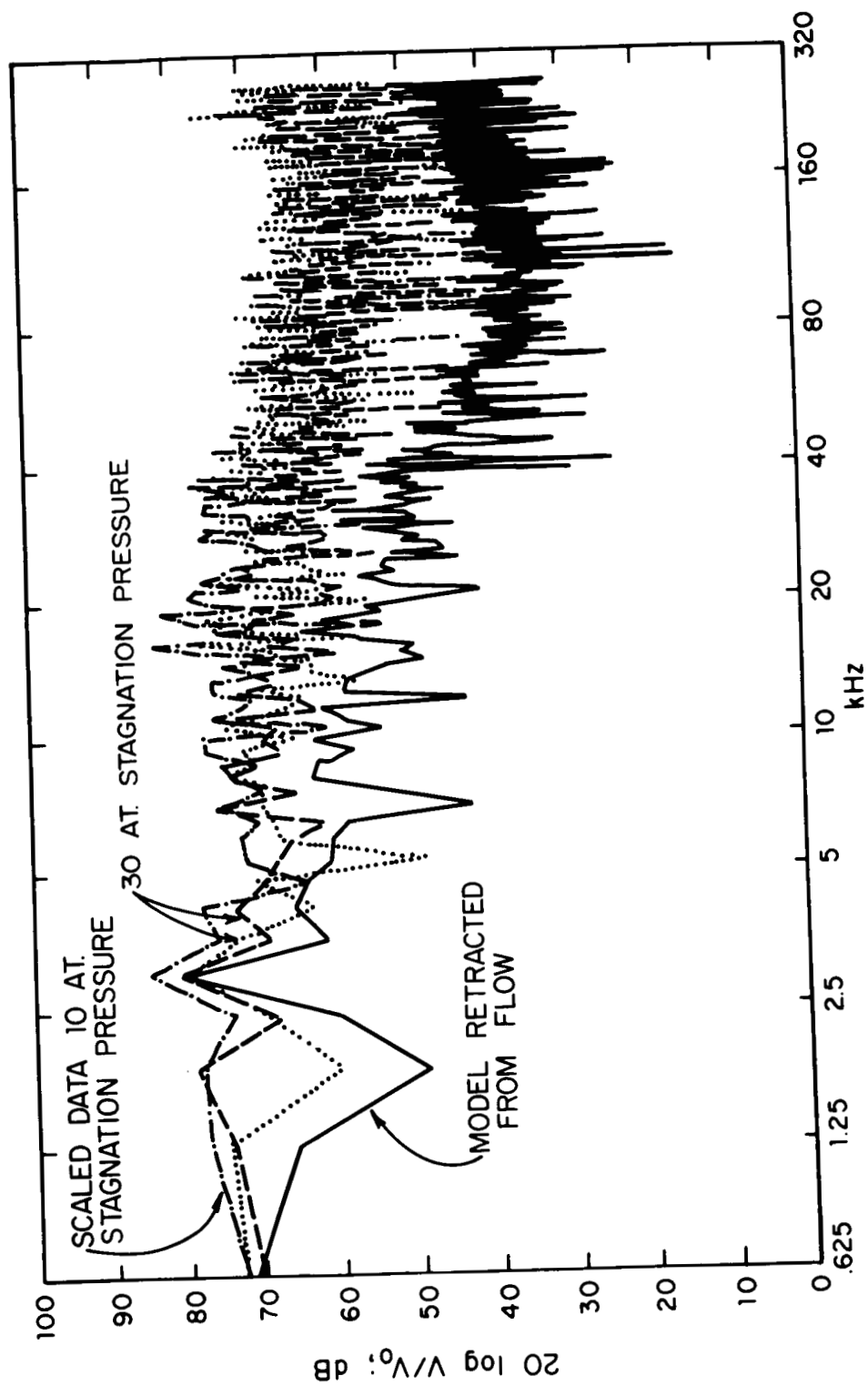section (within the flow field) does not seem to change spectra

FIG. 16.   FLUCTUATING-PRESSURE LEVEL SPECTRUM OBTAINED THROUGH SENSOR NO. 3 ON APEX OF CONE MODEL IN H-3 FACILITY AT MACH 6:   RAW DATA

markedly. Retracting the model from the flow (see Fig. 11) lowers the levels by 20 to 30 dB. The data obtained at lower stagnation pressure scales well with the other data; this indicates that this background noise spectrum results from nozzle wall turbulent boundary-layer radiation. Figure 17 shows similar data for sensor No. 5, located under the attached turbulent boundary layer near the base. Normalizing the rms pressures with the local dynamic pressure q_c allows direct comparison of the data (see Fig. 18). In Fig. 18, a best-fit line is drawn through each data range, and levels above 100 kHz were corrected for sensor sensitivity. Converting the constant-absolute bandwidth spectrum into a 1/3-octave band spectrum allows direct comparison with data obtained previously in the MIT tunnel at Mach 4 (Fig. 19). Although the mean spectrum for sensor No. 3 is about 5 to 8 dB below the sensor No. 5 spectrum in the 2.5- to 40-kHz frequency range, the two spectra shapes are similar. Sensor No. 5 levels exceed sensor No. 3 levels substantially only above 60 kHz. This implies that below 60 kHz signals are due to tunnel background noise; above that, sensor No. 5 measures TBL pressure fluctuations. Figure 19 supports this conclusion where "MIT Mach 4 data" is compared to "VKI Mach 6 data". Because of the thinner boundary layer and the higher flow speed, the spectral peak for the Mach 6 data is much higher and is estimated to be near 450,000 Hz. The above figure in Fig. 19 shows the Mach 4 and the Mach 6 1/3-octave band spectra in seminormalized form. Here, $20 \log (p_{rms}/q_e)$ is plotted vs real frequency. The lower figure shows both spectra fully nondimensionalized: $20 \log p_{rms}/q_e$ is plotted vs Strouhal number $S \equiv f\delta/U_e$, where f is the 1/3-octave band center frequency, δ is the boundary-layer thickness, and U_e is the flow speed on the cone. The implication is that below $S \approx 0.1$, the spectra are attributable to tunnel background noise in both cases. Of course, it is not expected that
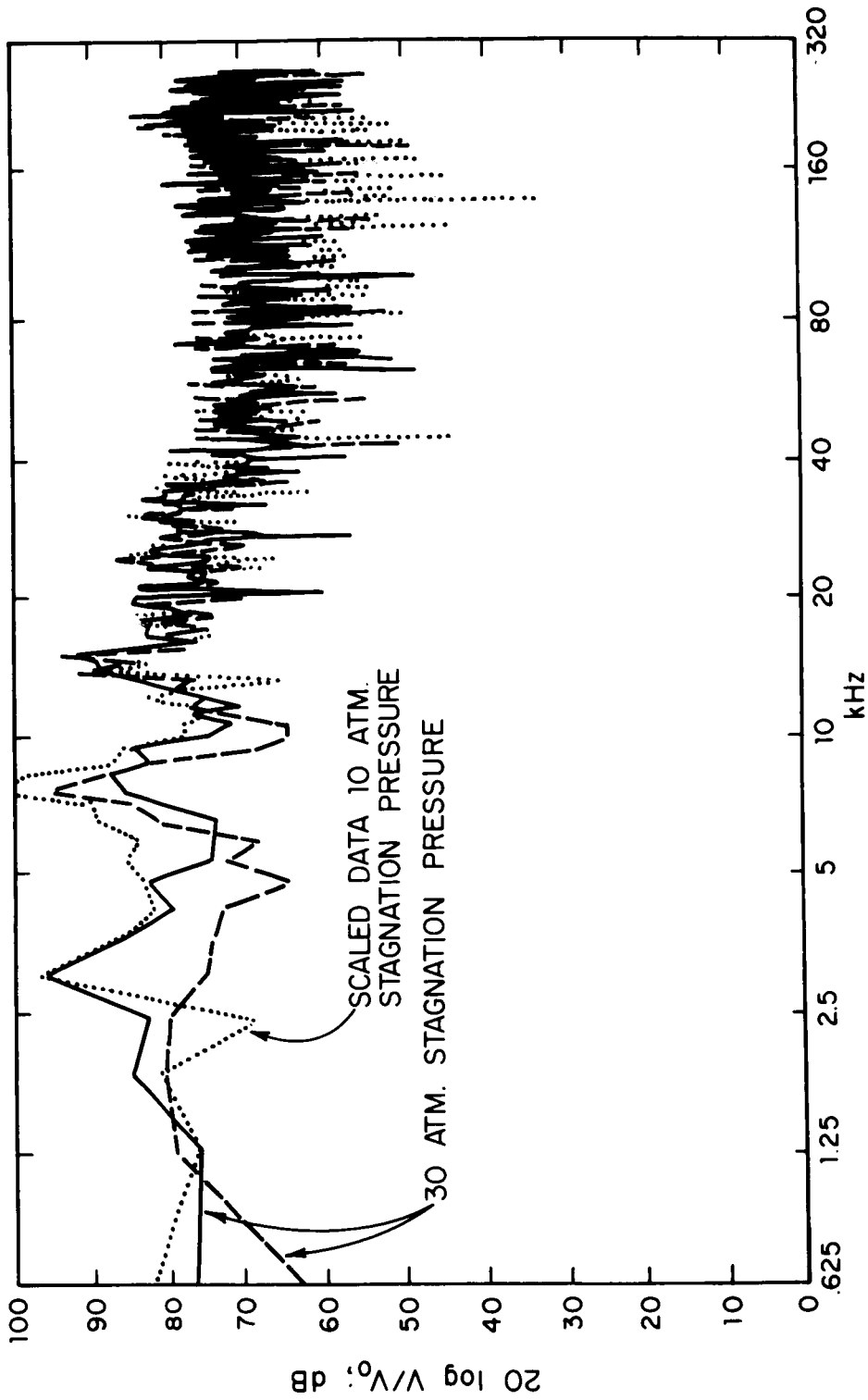
FIG. 17. FLUCTUATING-PRESSURE LEVEL SPECTRUM OBTAINED THROUGH SENSOR NO. 5 ON THE REAR CONE SURFACE IN H-3 FACILITY AT M_∞ = 6: RAW DATA
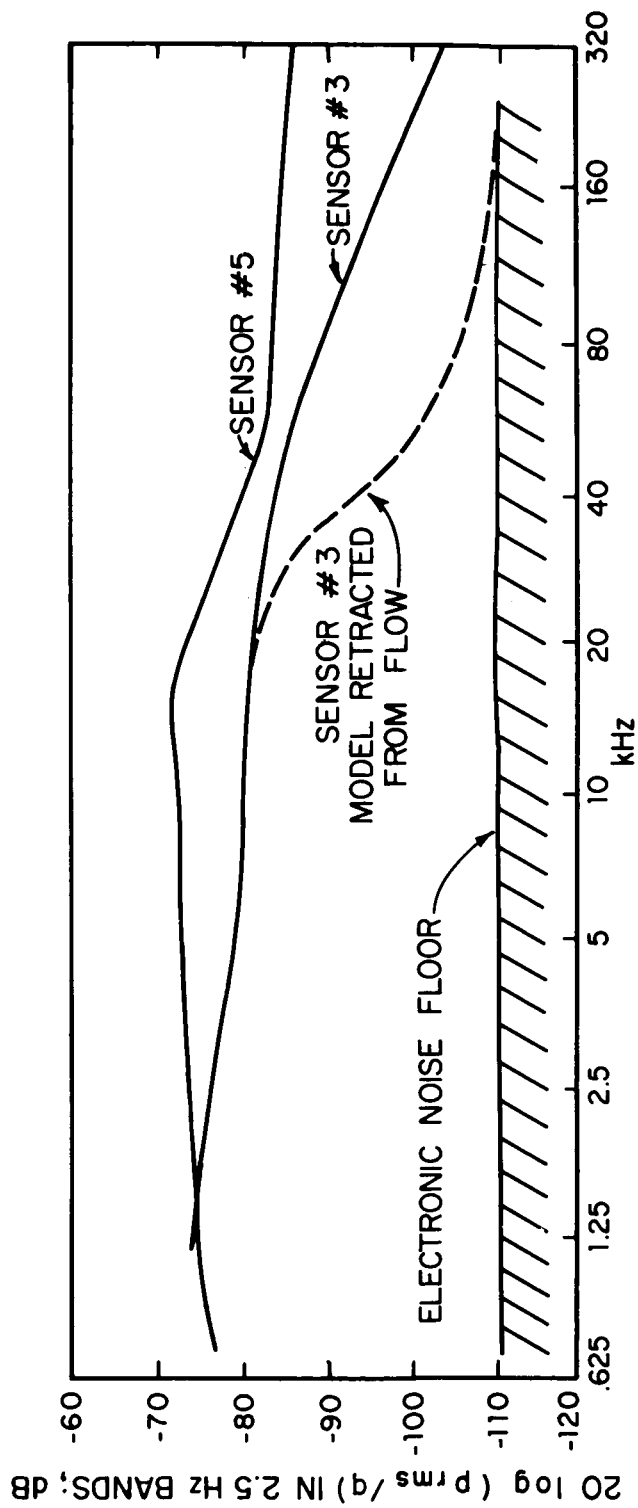
FIG. 18. SEMINORMALIZED REPRESENTATION OF FLUCTUATING-PRESSURE SPECTRA OBTAINED FROM SENSOR NO. 3 (UNDER LAMINAR BL) AND SENSOR NO. 5 (UNDER TURBULENT BL) ON CONE SURFACE AT $M_\infty = 6$
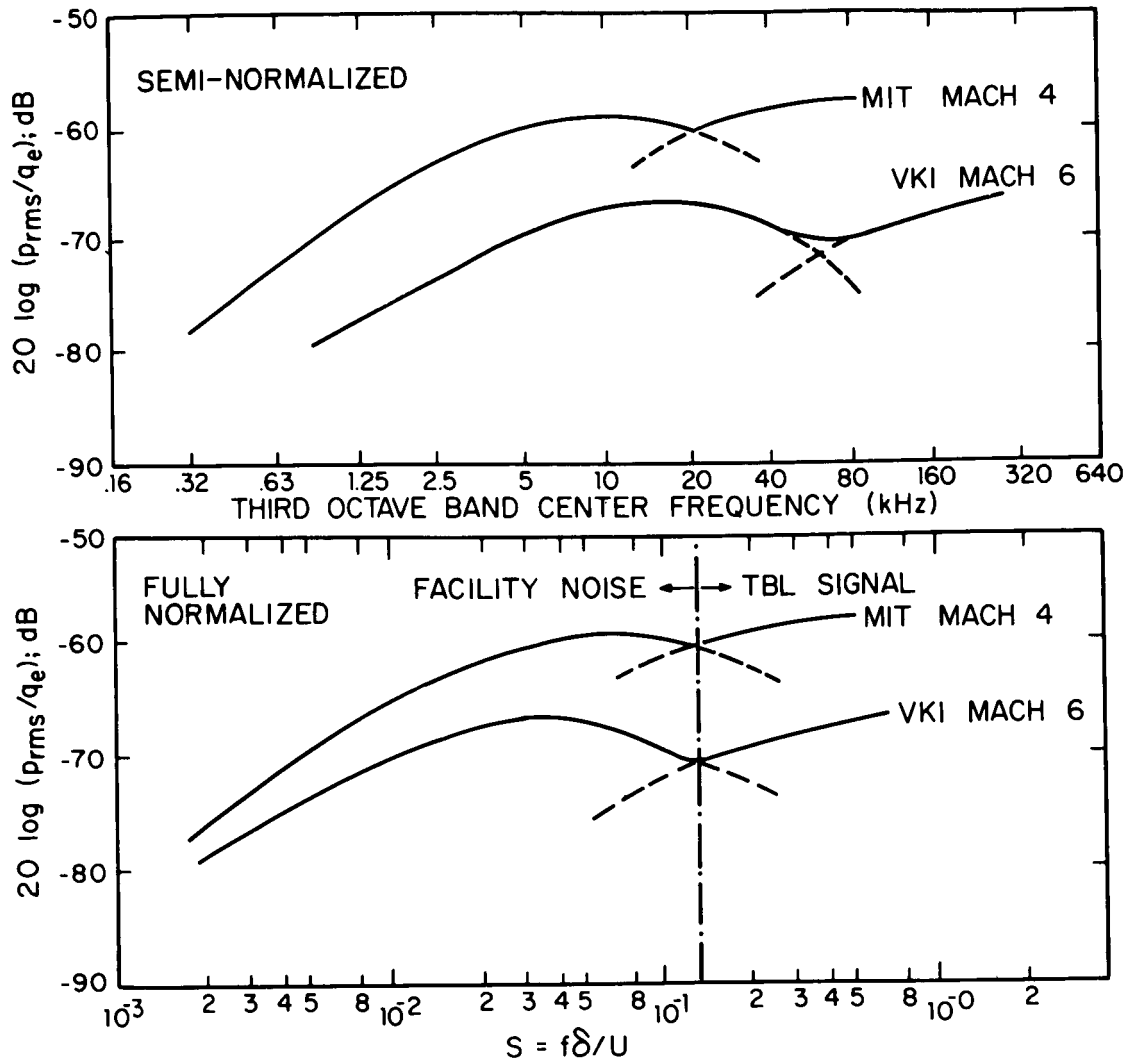
FIG. 19.   COMPARISON OF FLUCTUATING-PRESSURE SPECTRA
OBTAINED IN THE MIT TUNNEL AT $M_\infty = 4$ AND THE
VKI H-3 TUNNEL AT $M_\infty = 6$

36

tunnel noise spectra from different facilities and different
Mach numbers scale with each other; thus, the spectra below
S ≈ 0.1 should not be compared. The portion of the spectra above
S ≈ 0.1, however, is due to turbulent boundary-layer fluctuations
and can be compared on the basis of the nondimensionalization.

A nondimensional attached turbulent boundary-layer spectrum
referenced to the overall level is presented by K. Chandiramani,
et al (1966). Thus, the overall levels of a TBL-spectrum can be
derived from only a portion of that spectrum. Since the spectral
levels have been measured in a Strouhal number range from 0.1 to
0.5, the overall levels of the spectra under consideration can
be accurately estimated. Figure 20 shows overall relative
fluctuating-pressure levels vs Mach number including data from
Coe and Chyu (1972), Martelucci, Chaump, and Smith (1972), Heller
and Holmes (1971), and the present study.

All data points from M=0 to M=8 with the exception of one
point at Mach 4 lie within a ±3 dB band of a best-fit curve, which
can be represented as

$$\left(\frac{P_{rms}}{q}\right)_{overall} = \frac{0.0055}{1 + (0.22M)^2} \tag{1}$$

This equation will be modified later in this report to accommo-
date the high Mach-number data points.

2. *Base data*. Figures 21 and 22 depict fluctuating-pressure
level (FPL) spectra from sensors No. 7 and No. 8, respectively. In
both cases, the sensor resonance near 40 kHz shows quite clearly.

37

$$p_{rms}/q = \frac{0.0055}{1 + 0.05\,M^2}$$

Legend:
▲ COE et. al. (1972)
● HELLER et. al. (1971)
○ MARTELLUCCI (1972)
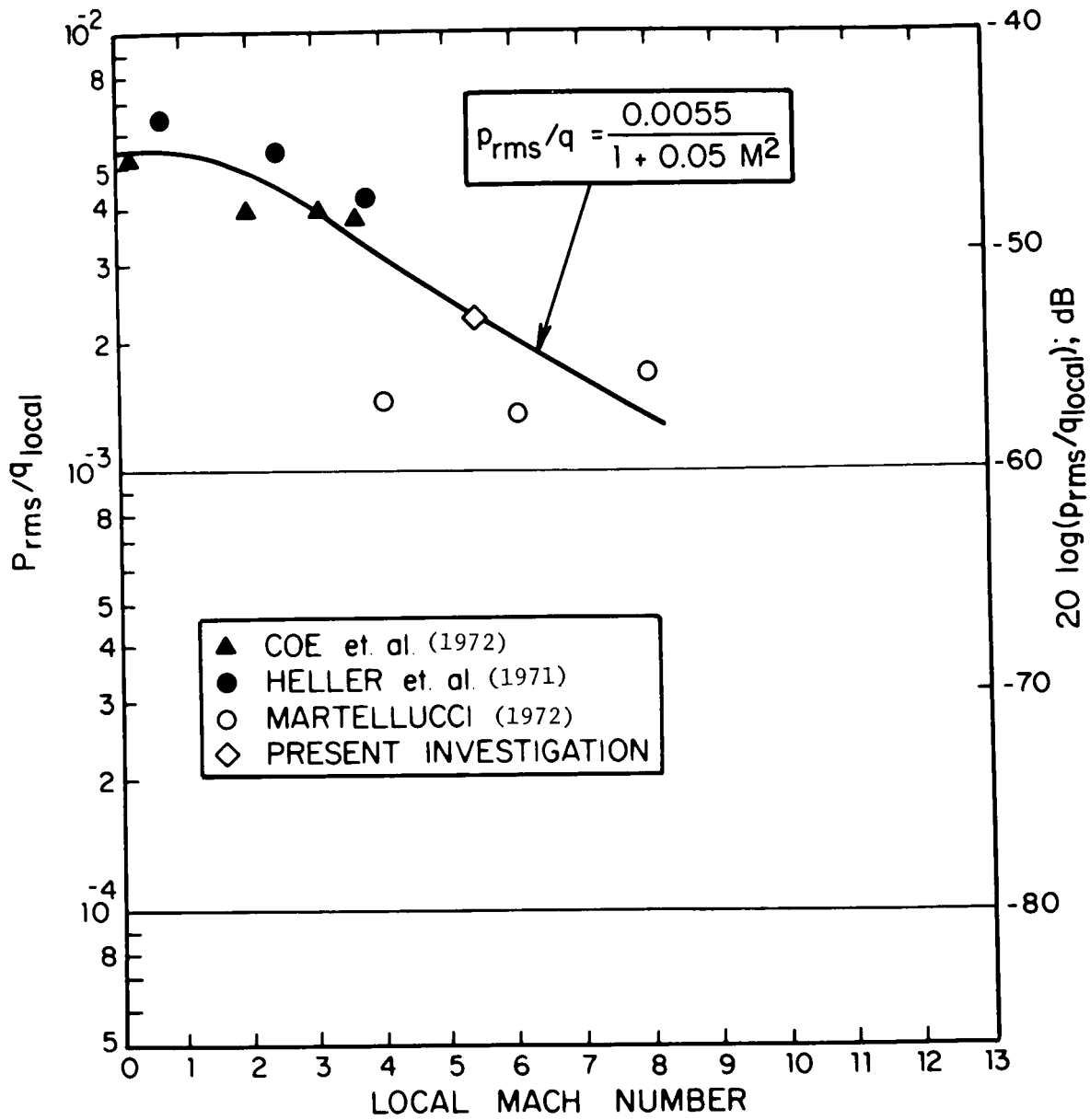◇ PRESENT INVESTIGATION

FIG. 20. MACH-NUMBER DEPENDENCE OF OVERALL FLUCTUATING-PRESSURE LEVEL UNDER ATTACHED TURBULENT-BOUNDARY LAYER
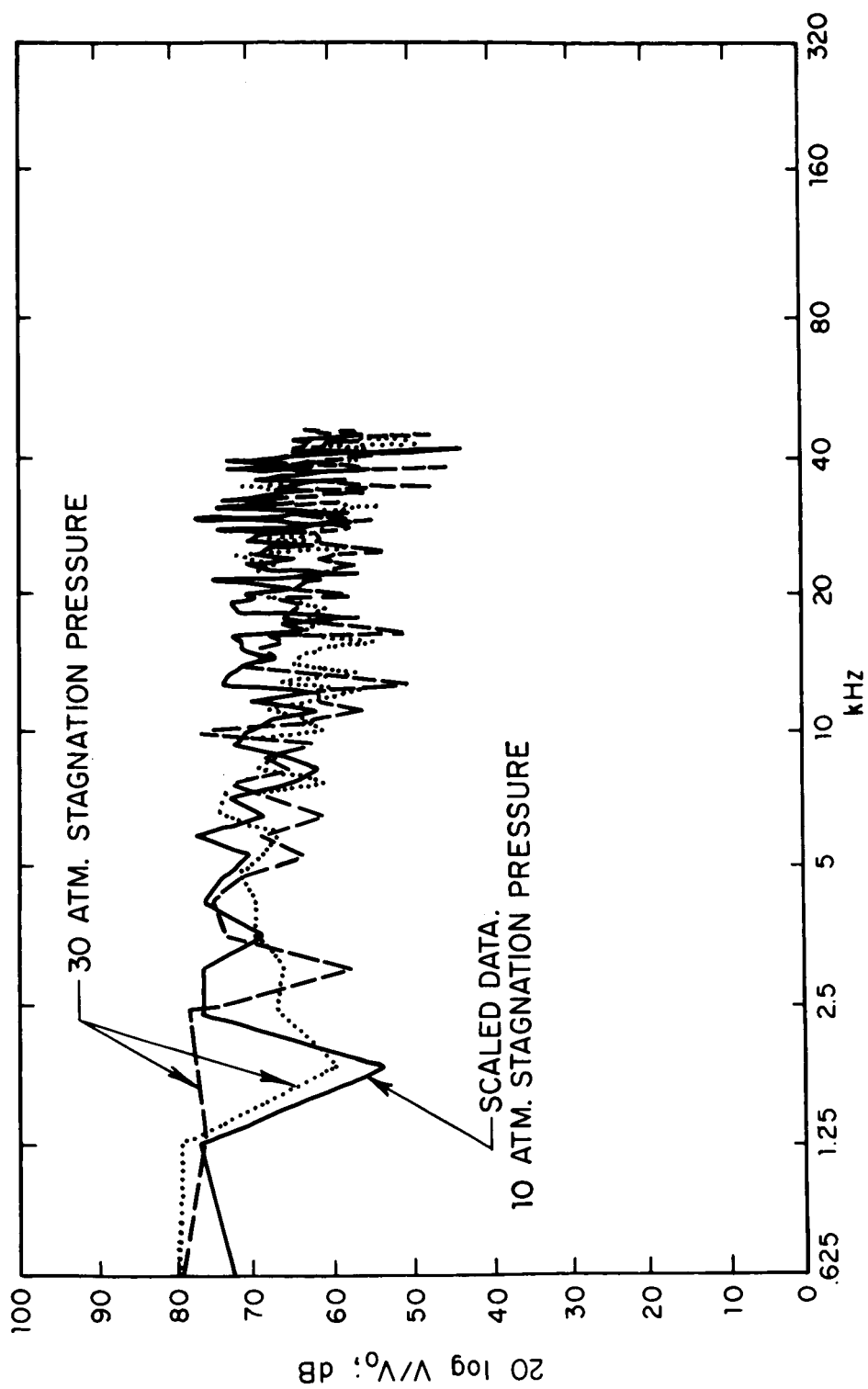
FIG. 21. FLUCTUATING-PRESSURE LEVEL SPECTRA OBTAINED THROUGH SENSOR NO. 7 ON THE BASE OF MODEL IN THE H-3 FACILITY AT $M_\infty = 6$: RAW DATA
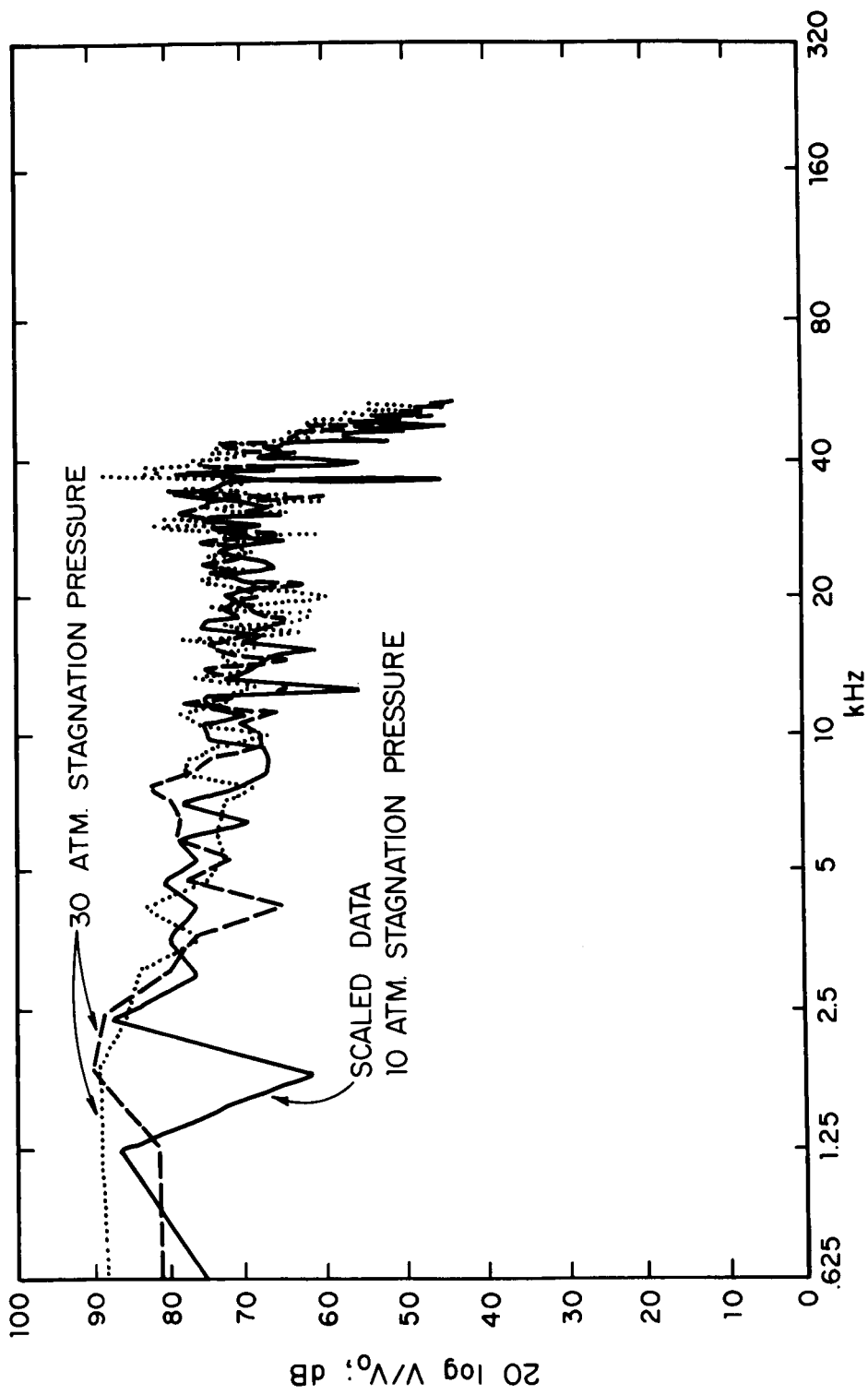
39

FIG. 22. FLUCTUATING-PRESSURE LEVEL SPECTRA OBTAINED THROUGH SENSOR NO. 8
ON BASE OF MODEL IN H-3 FACILITY AT $M_\infty = 6$: RAW DATA

40

Information above about 20 kHz cannot be used. It is worth noting
that the data for the low-Re-case scales perfectly, although the
entire flow over the model is quite likely laminar. Thus, it
evidently does not matter whether separated flow is laminar or
turbulent for similar pressure signals to be generated on the base.
Figure 23 shows the smoothed versions of the spectra, corrected
for sensor sensitivity above 10 kHz, and converted into nondimen-
sional 1/3-octave band spectra. Here, the Strouhal frequency em-
ploys the 1/3-octave band center frequency, the base diameter is
D, and the free-stream flow speed U_{∞}.

These spectra can be directly compared with those obtained
in the previous study (Heller and Holmes, 1971). Figure 24 shows
the Mach 6 base-pressure spectrum obtained from both the base
sensors. The average levels are about 8 dB below the Mach 4
levels, and the trend for (normalized) base pressures to decrease
with Mach number is quite obvious. The new information permits
the definition of a nondimensional base-pressure spectrum, ref-
erenced to the overall level, that utilizes data points obtained
at free-stream Mach numbers of 0.67, 2.5, 4, and 6. This spectrum
is shown in Fig. 25. The spectrum peaks at S = 0.15.

Figure 26 shows overall normalized base pressure vs Mach
number, employing test results by Eldred (1961), Widnall (1968),
Heller and Holmes (1971), and the present results. With reason-
able confidence, a curve can be fitted through these data points
at supersonic Mach numbers. However, the exact curve shape at
transonic speeds and subsonic speeds is doubtful since only two
data points are available. An empirical expression covering
these points can be written as:

$$20 \log (p/q) = 38 - 20 \log |M^2-1| \, . \qquad (2)$$

However, in the section entitled "Interpretation of Test Results,"
we will modify this expression to accommodate test results at
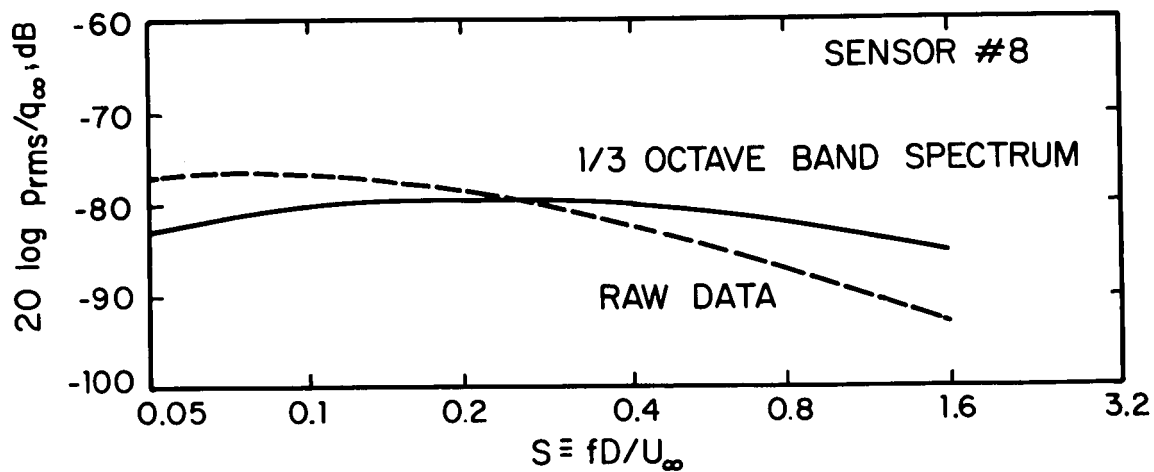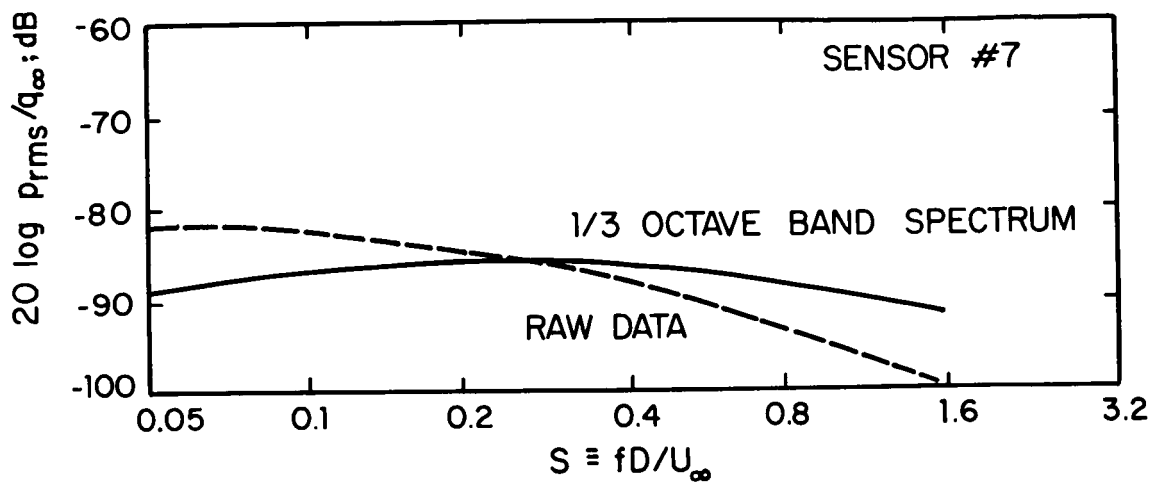higher Mach numbers.

FIG. 23. BASE-PRESSURE SPECTRA OBTAINED THROUGH SENSORS
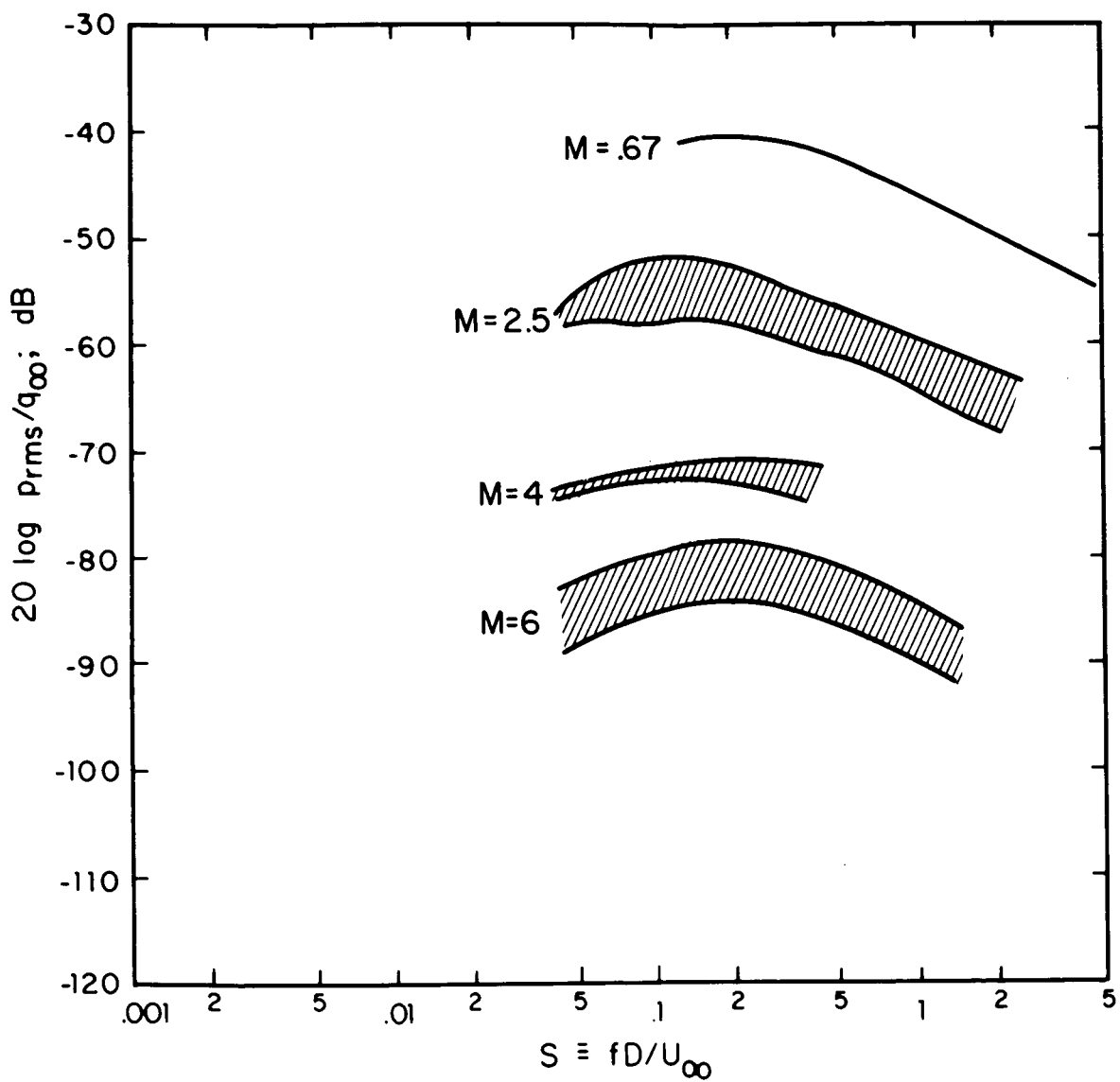NO. 7 AND NO. 8 IN H-3 FACILITY AT M_∞ = 6

FIG. 24. NONDIMENSIONAL BASE-PRESSURE SPECTRA FOR VARIOUS
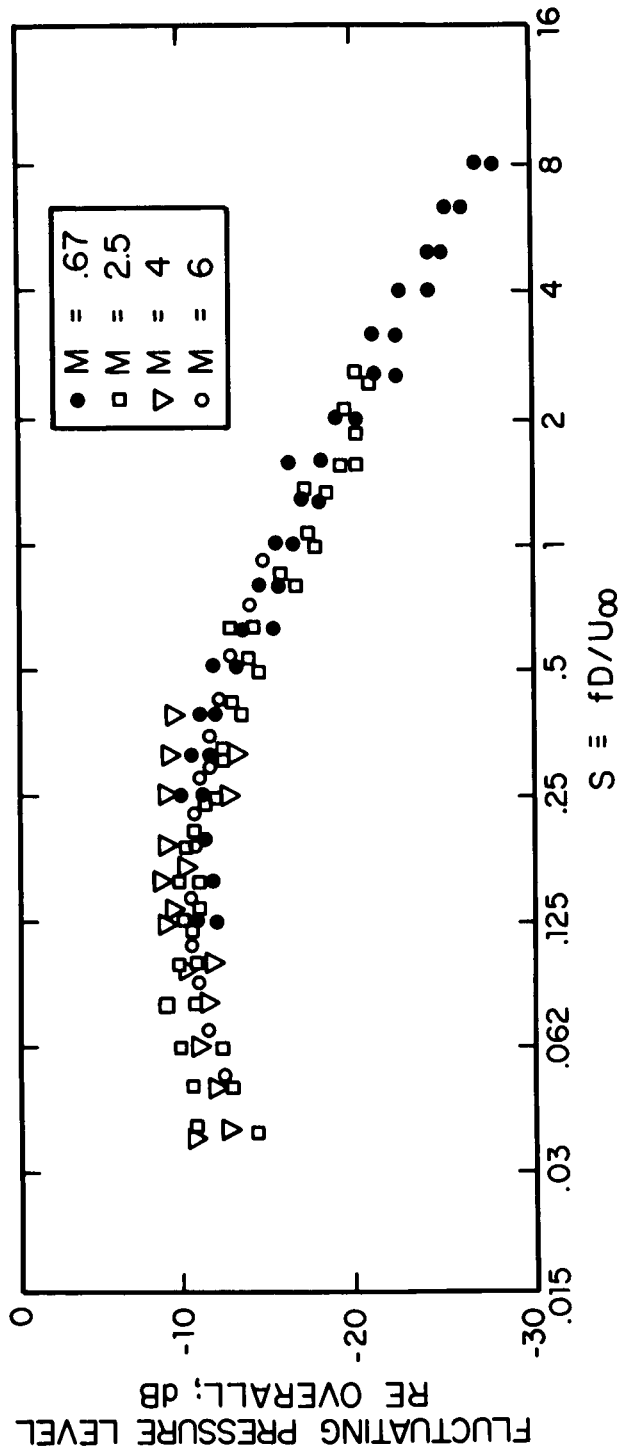FREE-STREAM MACH NUMBERS

FIG. 25. NONDIMENSIONAL BASE-PRESSURE SPECTRUM FOR SLENDER-CONE/FLAT-BASE BODIES IN FREE-STREAM FLOW AT MACH NUMBERS BETWEEN 0.67 AND 6
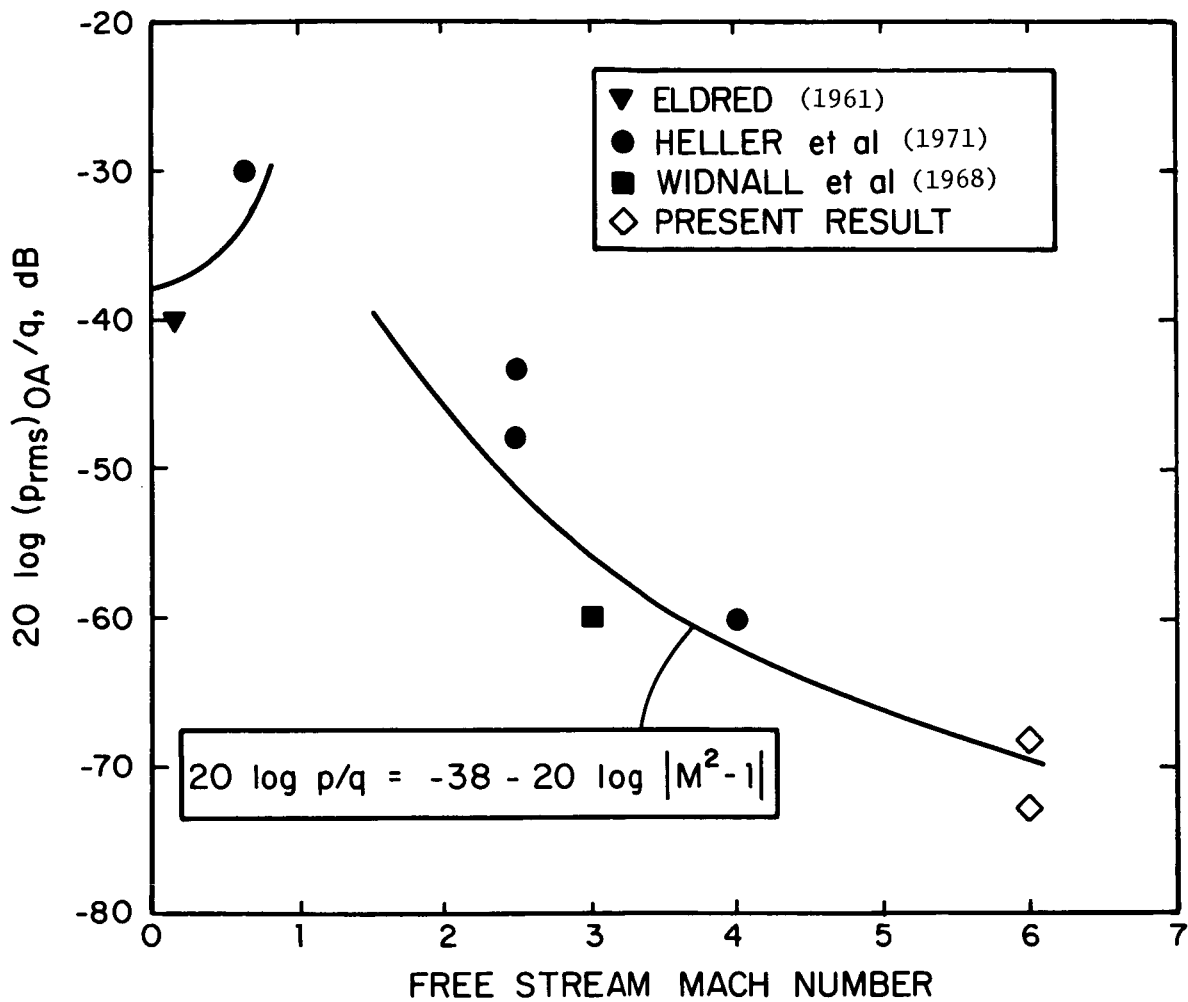
FIG. 26. FREE-STREAM MACH-NUMBER DEPENDENCE OF NORMALIZED
OVERALL BASE-PRESSURE LEVEL FOR SLENDER-CONE/FLAT-
BASE CONFIGURATIONS

Of course, this function goes to infinity at M=1. Thus, a
"damping-factor" at M=1 must be introduced as transonic data be-
comes available.

Mach-15 tests

Sensor Location

Figure 27 shows the sensor locations. Two heat transfer
gauges, two 1/10-in. sensors near the apex and two at the rear
of the cone, and five 1/4-in. sensors on the base are flush-
mounted within the surface contour.

Flow Conditions

The reservoir conditions upstream of the nozzle change
rapidly during a test run. Figure 28 depicts a typical time
history. There is a rapid pressure rise within approximately
2.5 msec up to a peak. Thereafter, pressure decays exponentially.
Typical decay conditions are:

Time After Peak (msec)	Stagnation Pressure atm (psia)	Stagnation Temperature (°K)	Unit Reynolds Number m^{-1} (ft^{-1})
0	4900 (72,070)	2810	19.8×10^6 (6×10^6)
2	3600 (53,000)	2560	16.5×10^6 (5×10^6)
4	2750 (40,450)	2350	13.0×10^6 (4×10^6)
6	2150 (31,630)	2180	11.5×10^6 (3.5×10^6)

After the pressure peak occurs in the reservoir chamber, the flow
reaches the model in about 1 msec. Then the starting shock passes
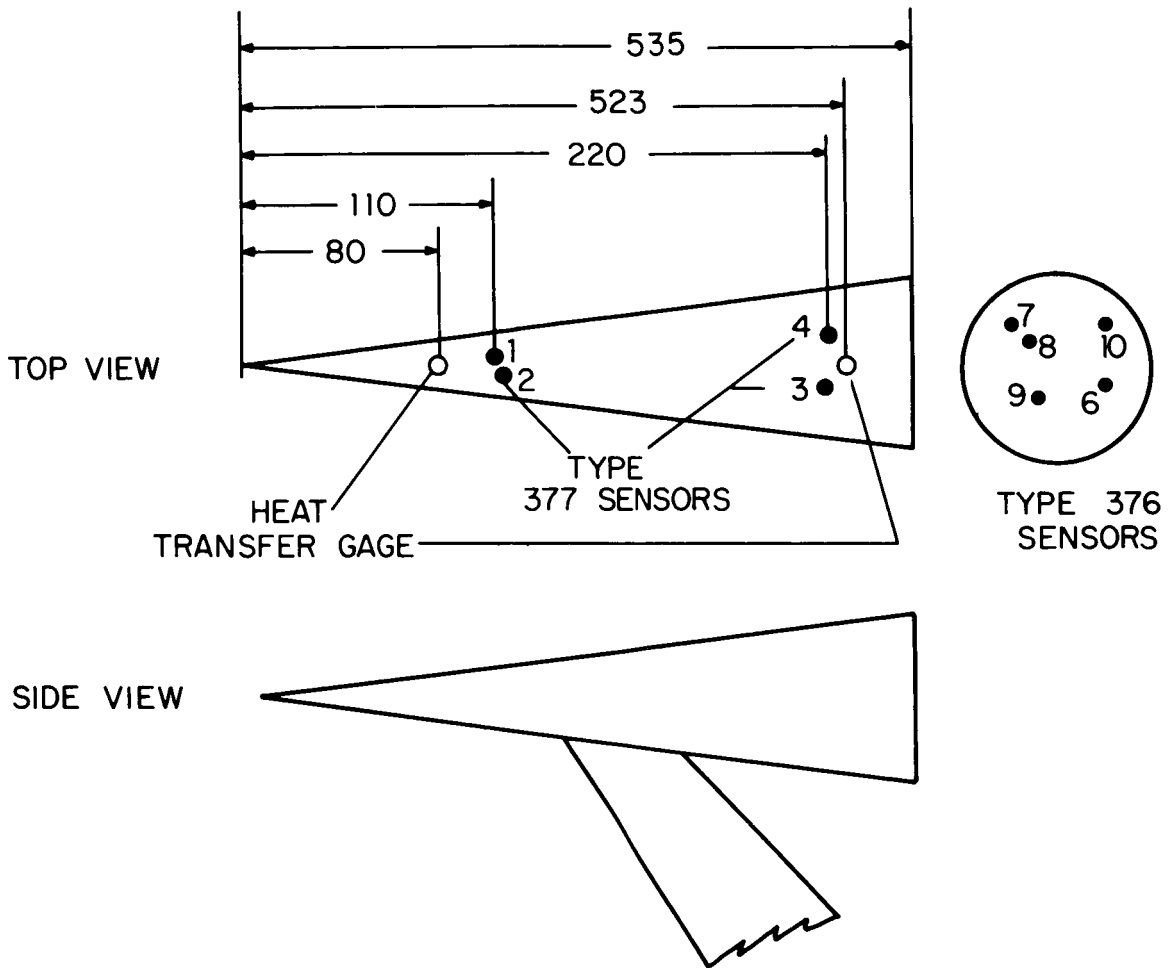over the model, and clean flow is established on the cone surface;

46

FIG. 27. SENSOR LOCATIONS ON MODEL IN LONGSHOT FACILITY
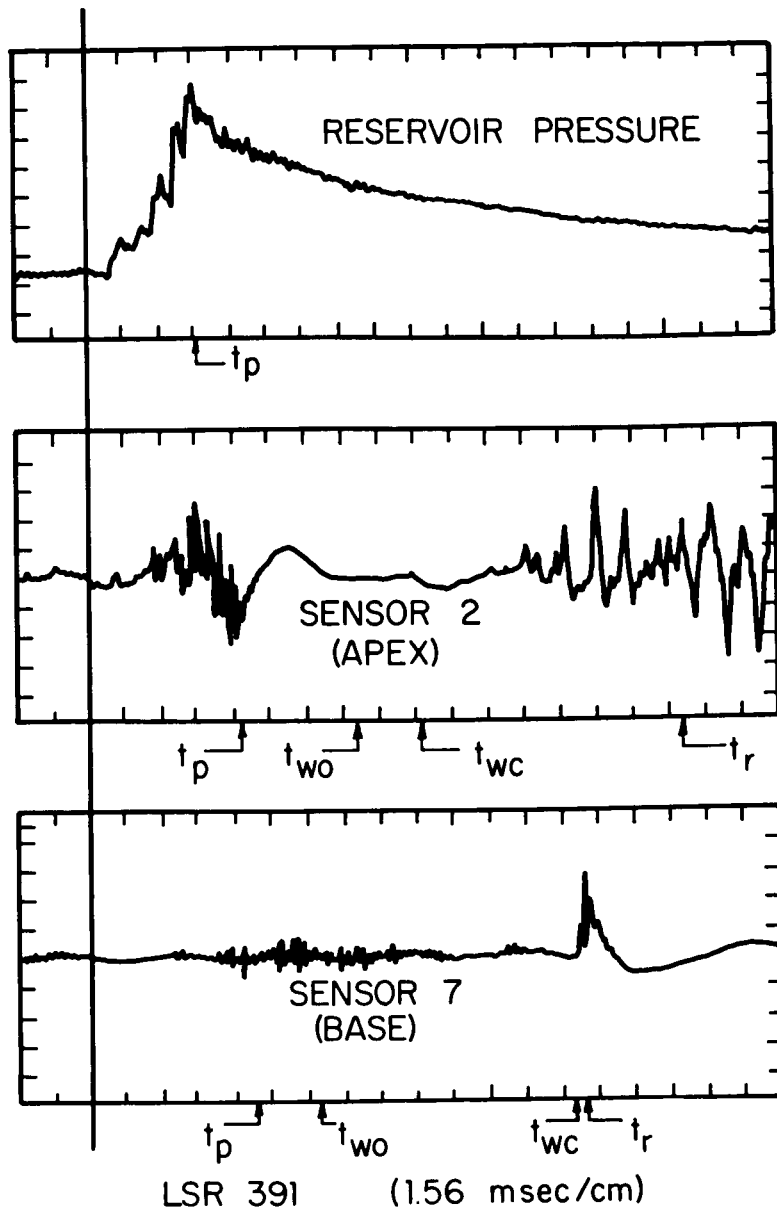(DIMENSIONS IN mm)

FIG. 28. TIME HISTORIES OF RESERVOIR PRESSURE AND TYPICAL
SENSOR SIGNALS ON EQUAL-TIME SCALE. t = occurrence
of event, Sufficies: p = pressure peak, wo = analysis
window open, wc = analysis window closed, r = reflected
wave

48

this may take another millisecond. To avoid analyzing fluctuating-pressure data at or near the ill-defined peak-stagnation pressure, data-analysis windows are further delayed by 1 msec. Thus, usually 3 msec are allowed to elapse after the reservoir chamber pressure peak occurs before sensor-signal windows are analyzed. Several delays are used, ranging from 3 msec to 4.5 msec; for the longest delays there was a possibility that the shock-wave, reflected from the test-chamber rear wall, had reached the model again. If this was evident, such data was discarded.

The following chart presents the flow conditions at the location of the apex- and rear-cone sensors for time after peak. Differences in Mach number at various stations are due to flow conicity.

APEX TRANSDUCERS

Time (msec) After Peak	M_∞	U_∞		q_∞		U_c		q_c	
		m/sec	ft/sec	atm	psf	m/sec	ft/sec	atm	lb/ft^2
0	14.7	2377	7800	1.267	2680	2359	7740	4.158	8800
2	14.4	2277	7470	1.02	2150	2249	7380	3.303	6990
4	14.3	2183	7163	0.834	1765	2158	7080	2.660	5630
6	14.1	2103	6900	0.685	1450	2076	6810	2.174	4600

REAR CONE TRANSDUCERS

Time (msec) After Peak	M_∞	U_∞		q_∞		U_c		q_c	
		m/sec	ft/sec	atm	psf	m/sec	ft/sec	atm	lb/ft^2
0	14.7	2377	7800	0.817	1730	2371	7780	2.174	4600
2	14.4	2277	7470	0.652	1380	2263	7424	1.729	3660
4	14.3	2183	7163	0.534	1130	2170	7120	1.394	2950
6	14.1	2103	6900	0.442	935	2088	6850	1.134	2400

Reynolds numbers on the cone surface based on the distance from the cone tip to the sensor locations are:

Time After Peak (msec)	Reynolds Number	
	Apex Sensors	Rear Cone Sensors
0	1.5×10^6	10×10^6
2	1.25×10^6	8.3×10^6
4	1×10^6	6.8×10^6
6	0.9×10^6	5.9×10^6

Reliable information on transition Reynolds number at hypersonic speeds is unavailable. However, a comparison of oscilloscope traces of the apex sensors and the rear cone sensors indicates that the apex sensors were at a location of much less intense fluctuations (Fig. 29). Thus, the rear-cone sensor signals represent turbulent or, at least, transitional flow.
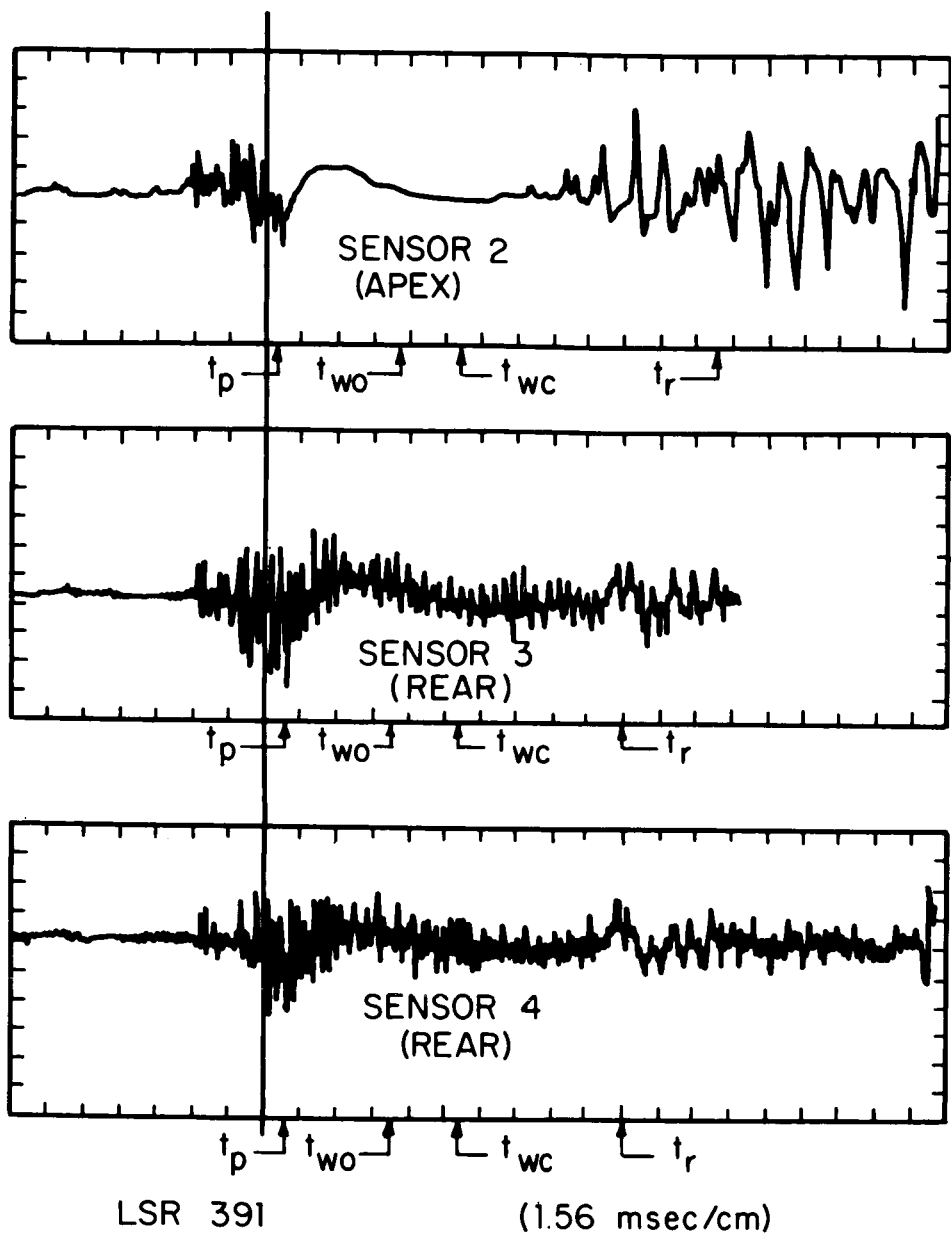
FIG. 29.   TIME HISTORIES OF CONE SENSOR SIGNALS UNDER LAMINAR
(SENSOR NO. 2) AND TURBULENT (SENSORS NO. 3 and NO. 4)
BOUNDARY LAYER ON MODEL IN LONGSHOT AT M_∞ = 15

51

Flow Visualization

Schlieren photographs indicate a fairly thick boundary layer on the rear cone surface; however, nothing reliable can be said about the stage of the boundary layer (Fig. 30). Boundary-layer thickness is estimated as 1/6-in. at the rear-cone sensor location.

Fluctuating-Pressure Measurements

1. Forward cone data. Figure 31 shows fluctuating-pressure level spectra obtained from sensors No. 2 and No. 3. Signal analysis begins 3 msec after the stagnation pressure peak and is conducted over a 1.6-msec time span. Corresponding data from sensor No. 4 is shown in Fig. 32. In Fig. 33, a best-fit line is drawn through the data points, and the spectra are converted into 1/3-octave band spectra.

In an analogous manner to the H-3 test data interpretation, it is postulated that the part of the spectra below about 50 kHz is facility background-noise related, and the part from 50 kHz to 250 kHz represents the cone-surface boundary-layer spectrum.

Figure 34 shows "sensors No. 3 and No. 4 spectra" in relation to the H-3 test data at Mach 6 and the earlier MIT test data at Mach 4. Facility noise in Longshot is relatively higher. The fully nondimensional representation (lower diagram in Fig. 34) indicates that the Mach 15 levels are 3 to 9 dB below the Mach 6 levels. Thus, the *overall* levels of the spectra should differ by the same amount.

Figure 35 is identical to Fig. 19, but it includes the data for free-stream Mach numbers of 15. Since local pressure spectra must be related to the local Mach number, the Longshot data points appear at $M_e = 12$, the Mach number on the cone surface.
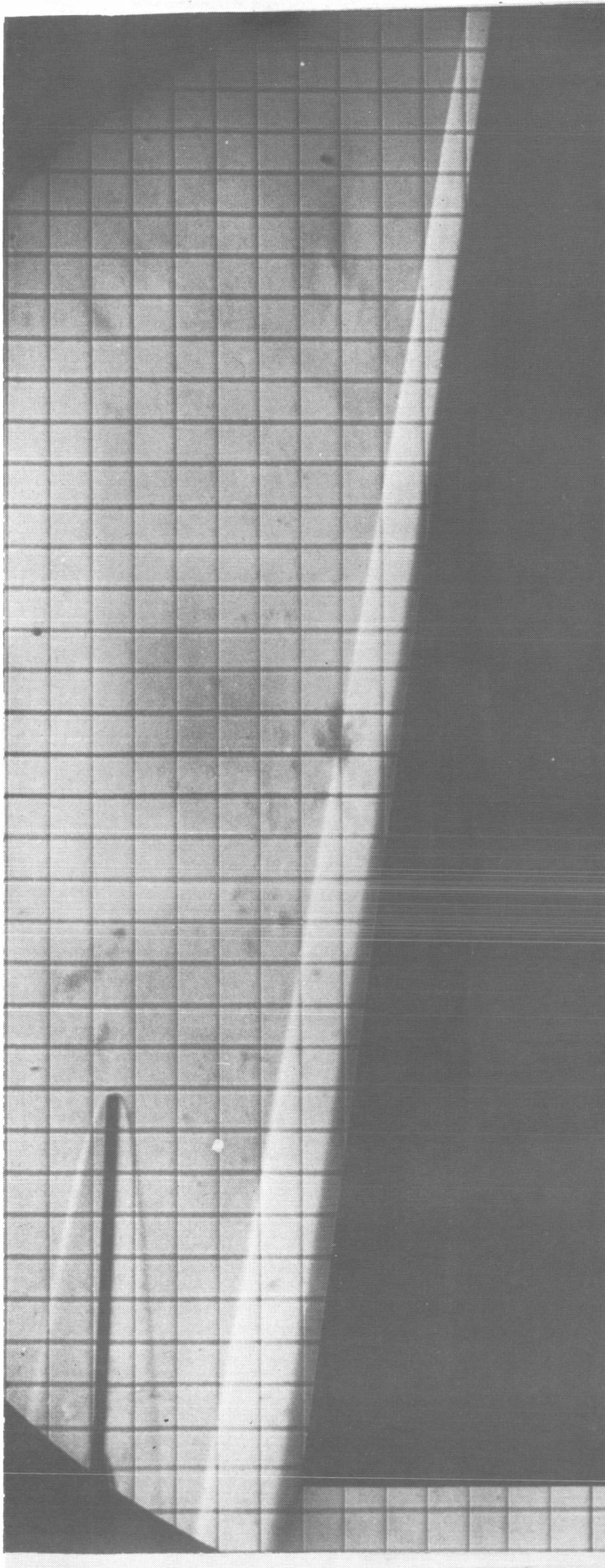
FIG. 30(a). SCHLIEREN OPTICAL FLOW VISUALIZATION OF FLOW OVER MODEL AT $M_\infty = 15$ (HIGH REYNOLDS-NUMBER CASE)
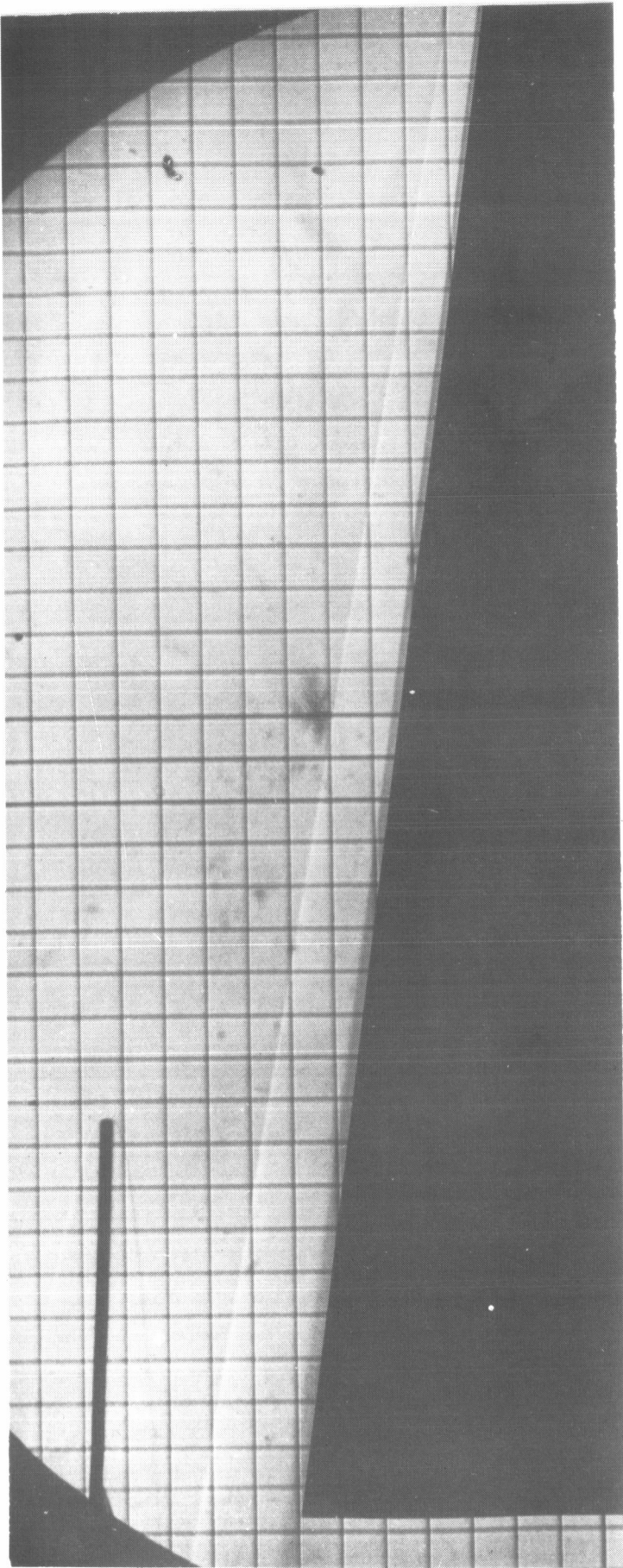
FIG. 30(b). SCHLIEREN OPTICAL FLOW VISUALIZATION OF FLOW OVER MODEL AT $M_\infty = 15$ (LOW REYNOLDS-NUMBER CASE)
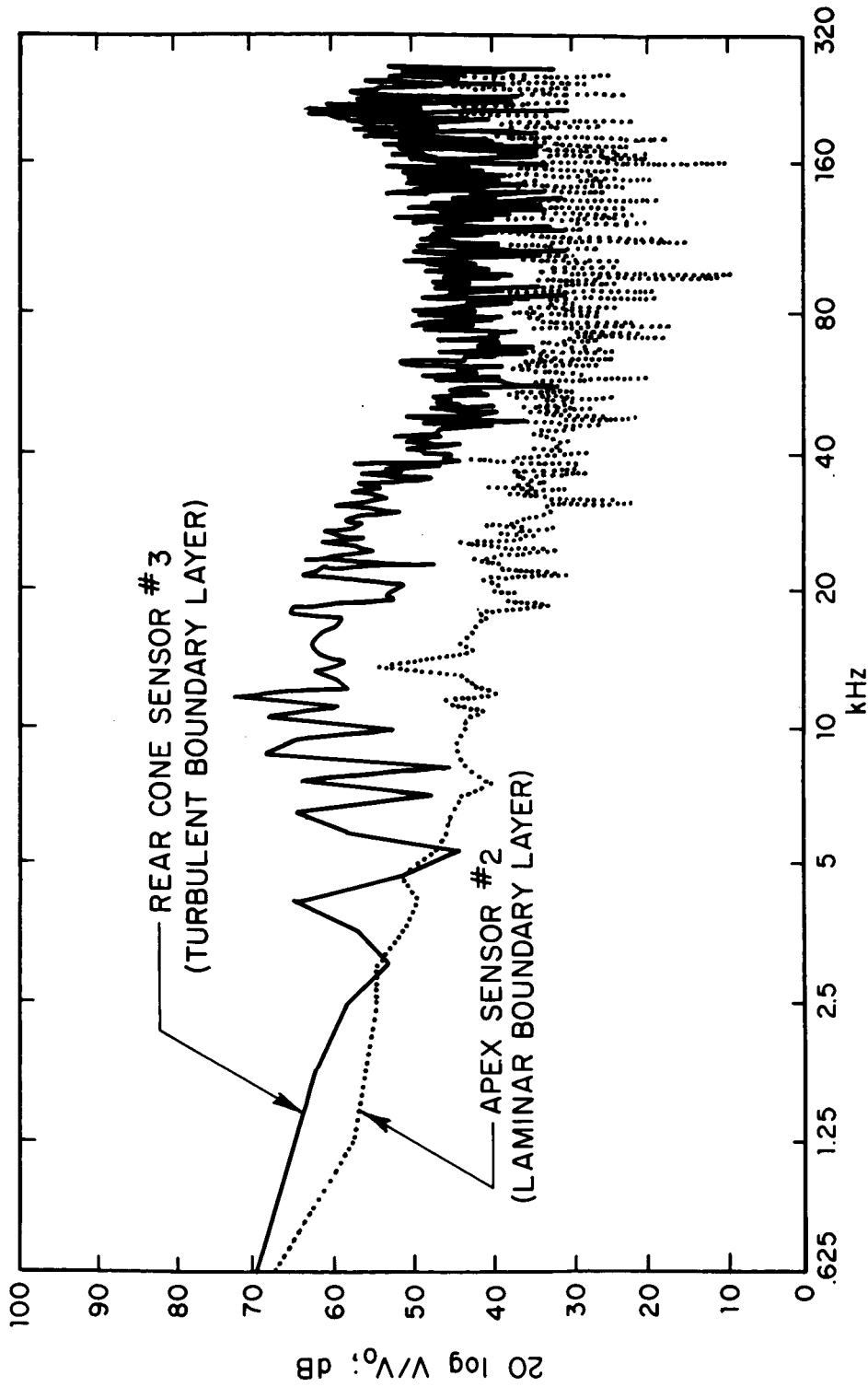
54

FIG. 31. FLUCTUATING-PRESSURE LEVEL SPECTRA OBTAINED THROUGH SENSOR NO. 3 UNDER TURBULENT BOUNDARY LAYER AND THROUGH SENSOR NO. 2 UNDER LAMINAR BOUNDARY LAYER ON THE MODEL IN THE LONGSHOT FACILITY AT MACH 15
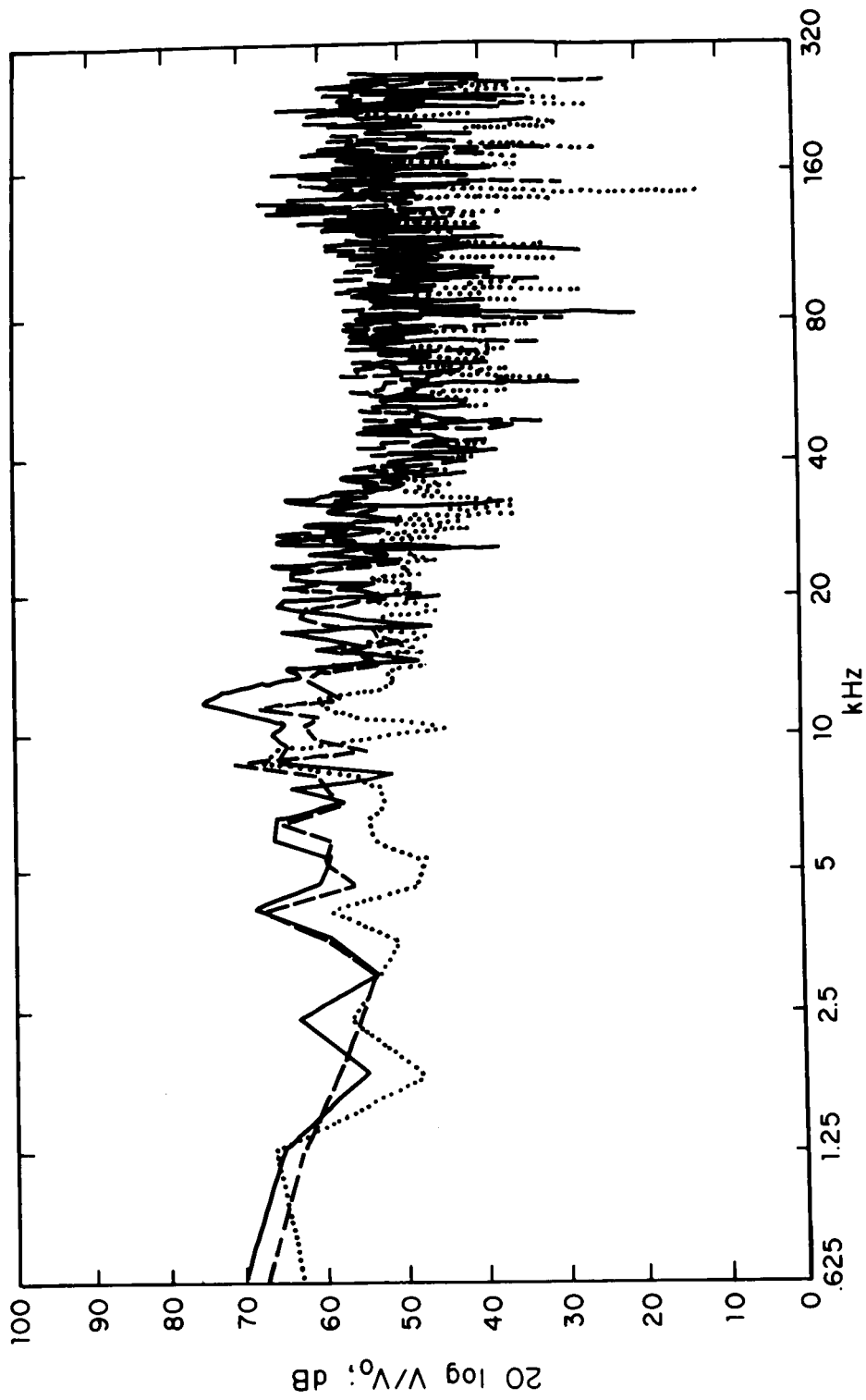
FIG. 32. FLUCTUATING-PRESSURE LEVEL SPECTRUM OBTAINED THROUGH SENSOR NO. 4
UNDER TURBULENT BOUNDARY LAYER ON THE MODEL IN LONGSHOT FACILITY
AT M_∞ = 15 (Different curves represent different runs)
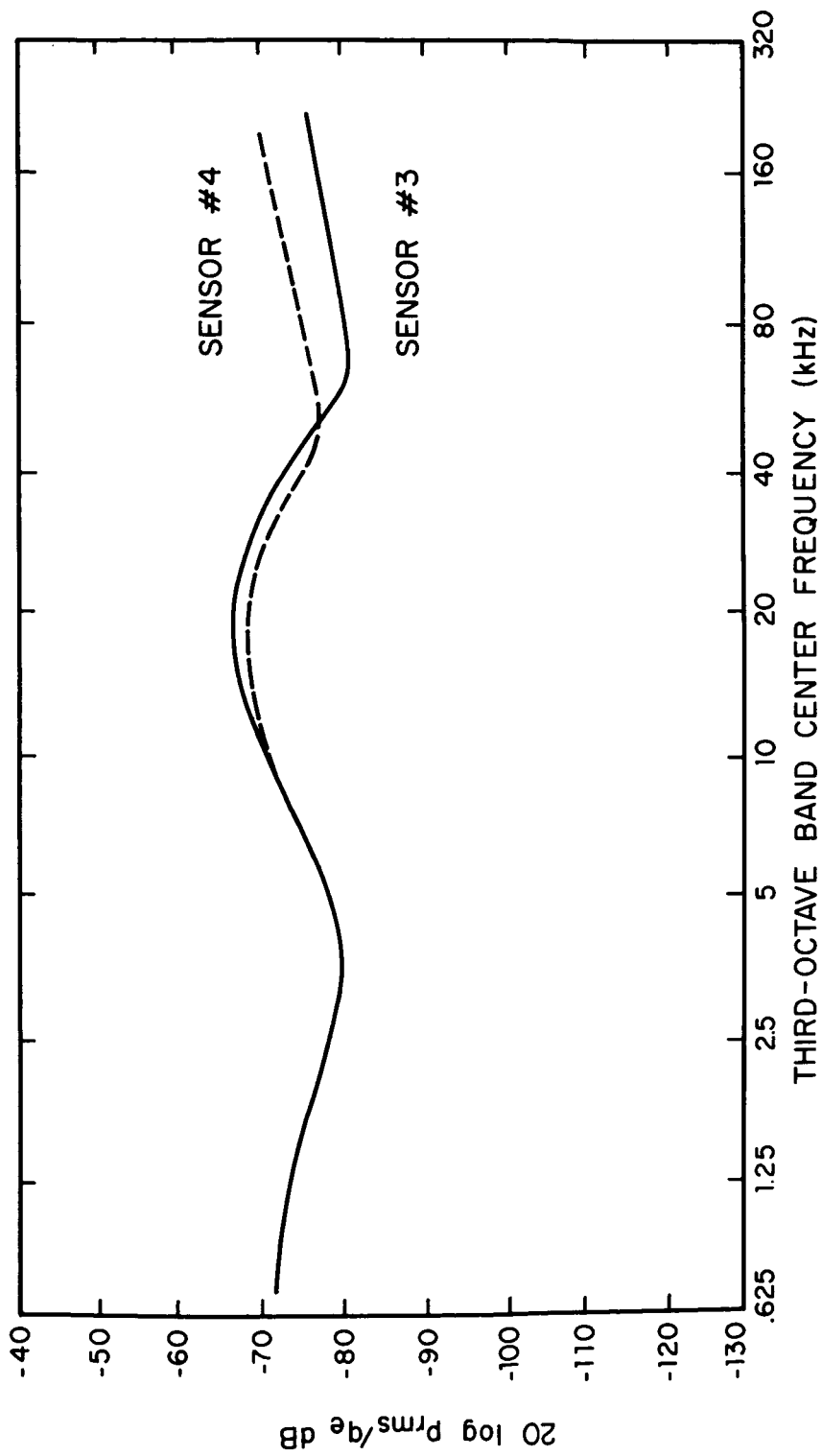
FIG. 33. SEMINORMALIZED PRESSURE SPECTRA OBTAINED THROUGH SENSORS NO. 3 AND NO. 4 ON CONE SURFACE OF MODEL IN LONGSHOT FACILITY AT M_∞ = 15
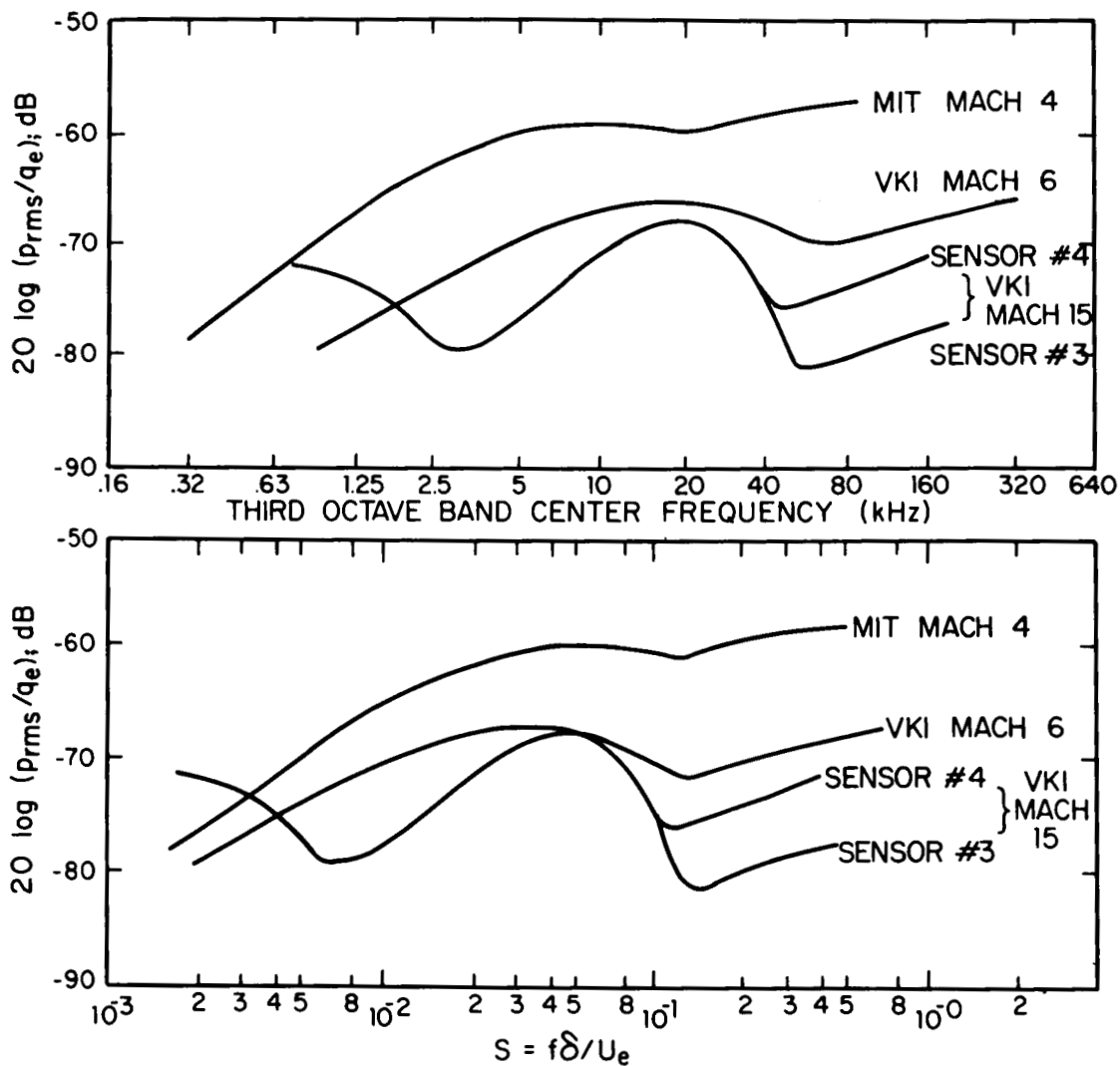
FIG. 34. COMPARISON OF TURBULENT BOUNDARY-LAYER SPECTRA OBTAINED
IN THE MIT TUNNEL AT $M_\infty = 4$, IN THE H-3 FACILITY AT
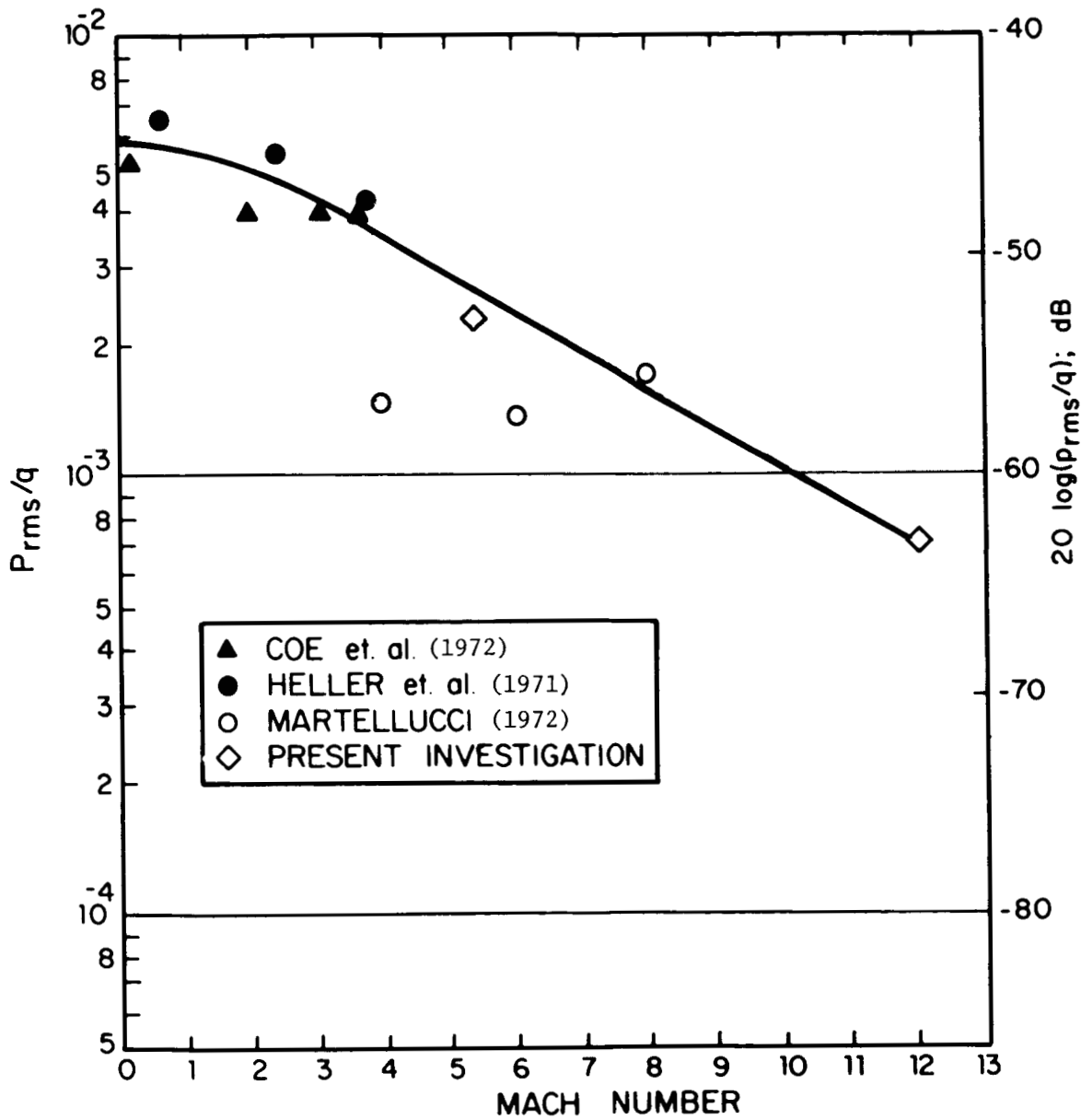$M_\infty = 6$, AND IN THE LONGSHOT FACILITY AT $M_\infty = 15$

FIG. 35. MACH-NUMBER DEPENDENCE OF OVERALL FLUCTUATING-PRESSURE
LEVEL UNDER ATTACHED TURBULENT BOUNDARY LAYER

2. *Base data.* Figure 36 shows data from sensors No. 7 and No. 8 analyzed after a 3.4-msec delay from reservoir peak. The spectra show two distinct shallow peaks: near 1.5 kHz and 13 kHz. The sharp drop above 40 kHz is because of the cutoff of analysis.

Figure 37 presents a best-fit curve through the data points, obtained through sensor No. 8, together with the corresponding 1/3-octave band spectrum. The smoothed sensor No. 7 spectrum shows a similar shape, with levels about 8 dB below those of sensor No. 8. If that part of the spectrum which peaks at 1.5 kHz is representative of the base-pressure spectrum, then its fully non-dimensional representation in the context of base-pressure spectra at lower Mach numbers indicates a continuous drop in levels with increasing Mach number (Fig. 38). Figure 39 shows the overall nondimensional levels for fluctuating base pressures as a Mach-number function; the Mach-15 data points are close to the previously proposed curve. Of course, some uncertainty is involved in drawing a "best-fit" curve through the data points shown in Fig. 36. Furthermore, there is no available explanation for the source of the "high-frequency" shallow peak. Its presence would raise the overall levels by more than 15 dB, and the spectrum peak would be located near a Strouhal number of 1 (for a 1/3-octave band representation), thus deviating from the pattern of the lower Mach-number spectra.

Comparison of data obtained from sensors located throughout the base plain at different Mach numbers allows the following conclusions on the intensity distribution.

Levels are highest near the rim of the base area, they decrease towards the base center, and increase again at the center. Probably, this is because of the impingement of highly turbulent recirculating flow in the center region. Figure 40 qualitatively illustrates this pattern.
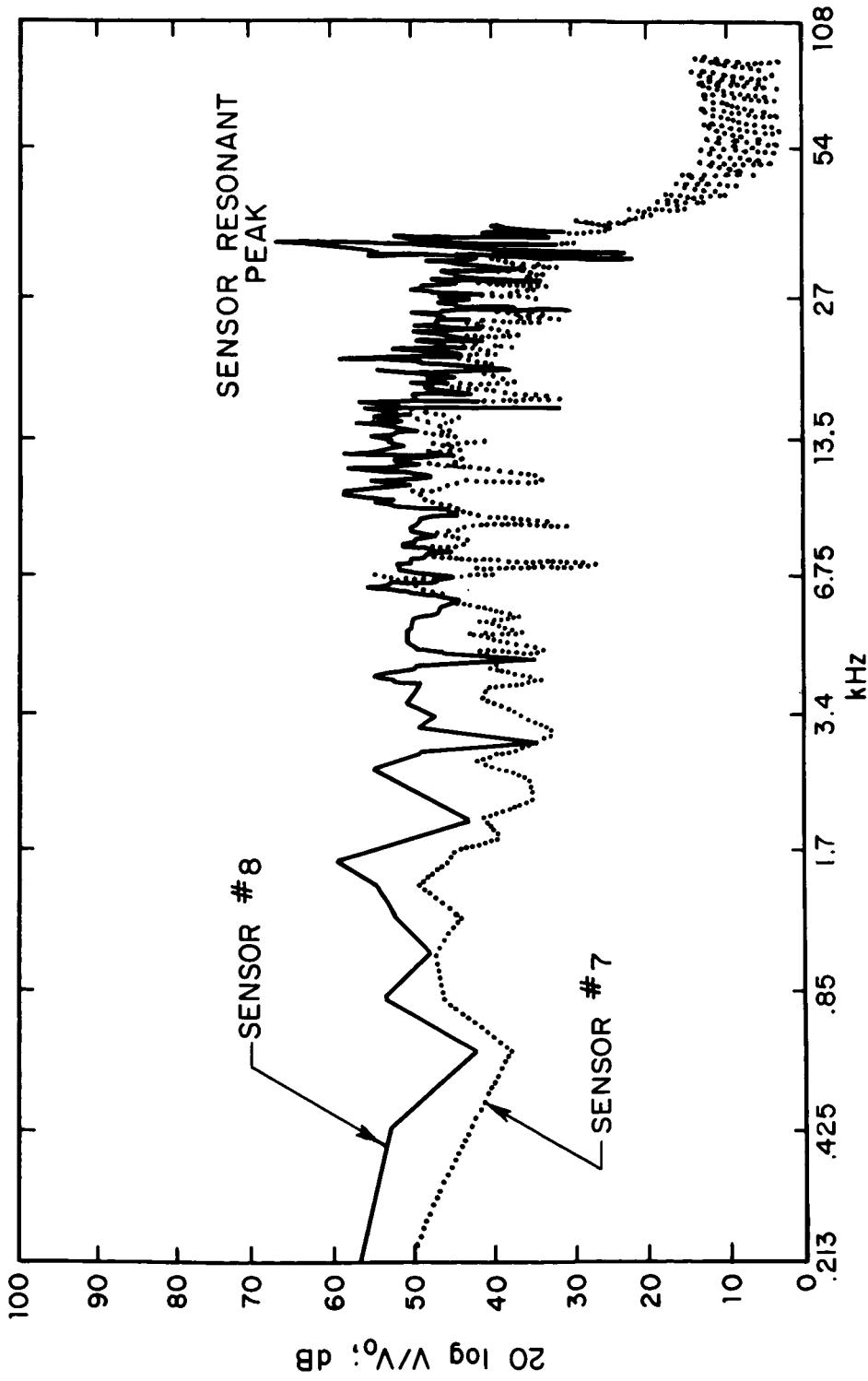
FIG. 36. FLUCTUATING BASE-PRESSURE SPECTRA OBTAINED THROUGH SENSORS NO. 7 AND NO. 8 ON THE MODEL IN LONGSHOT AT MACH 15: RAW DATA
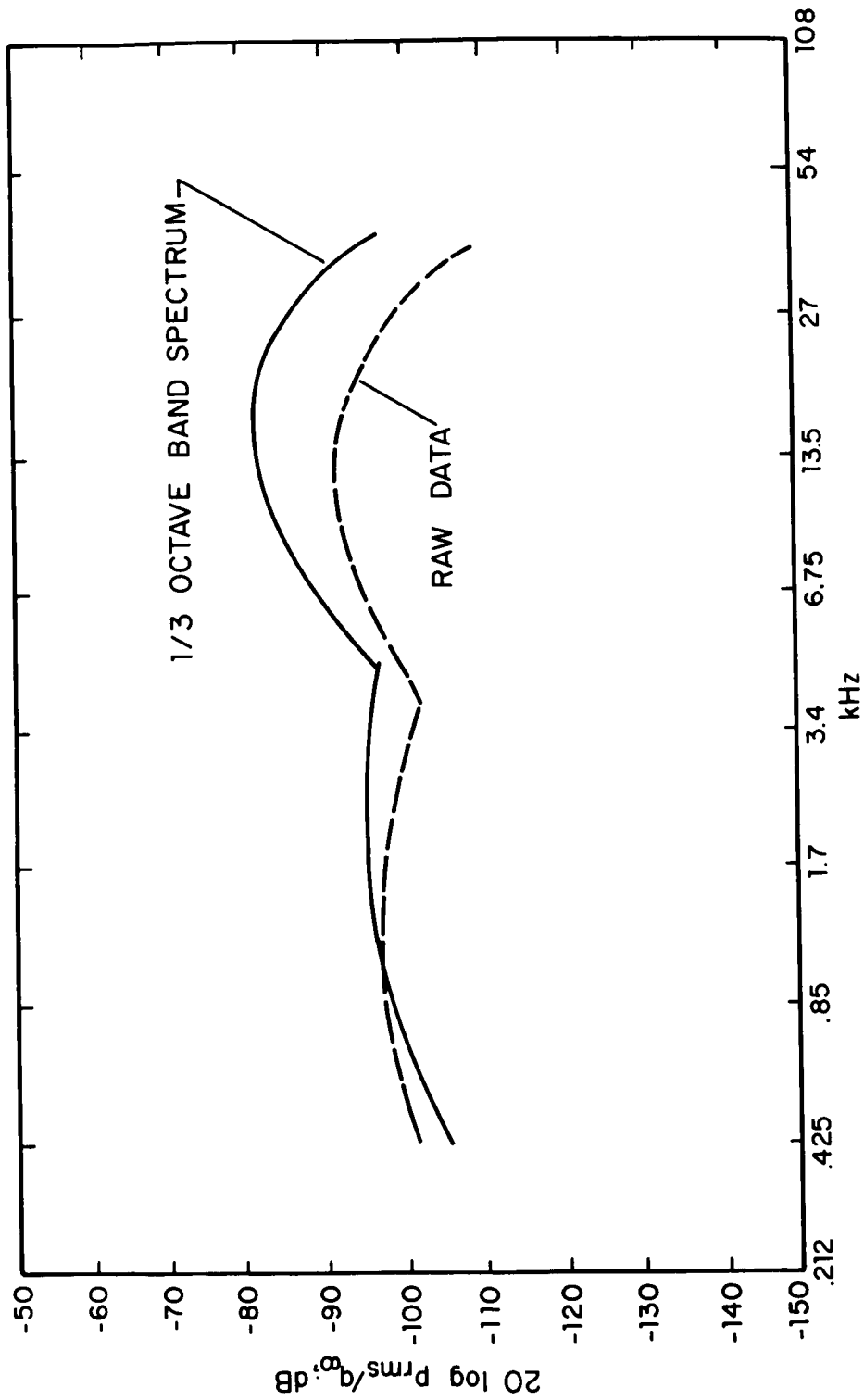
61

FIG. 37. SEMINORMALIZED BASE-PRESSURE SPECTRUM OBTAINED FROM SENSOR NO. 8 ON MODEL IN LONGSHOT FACILITY AT $M_\infty = 15$
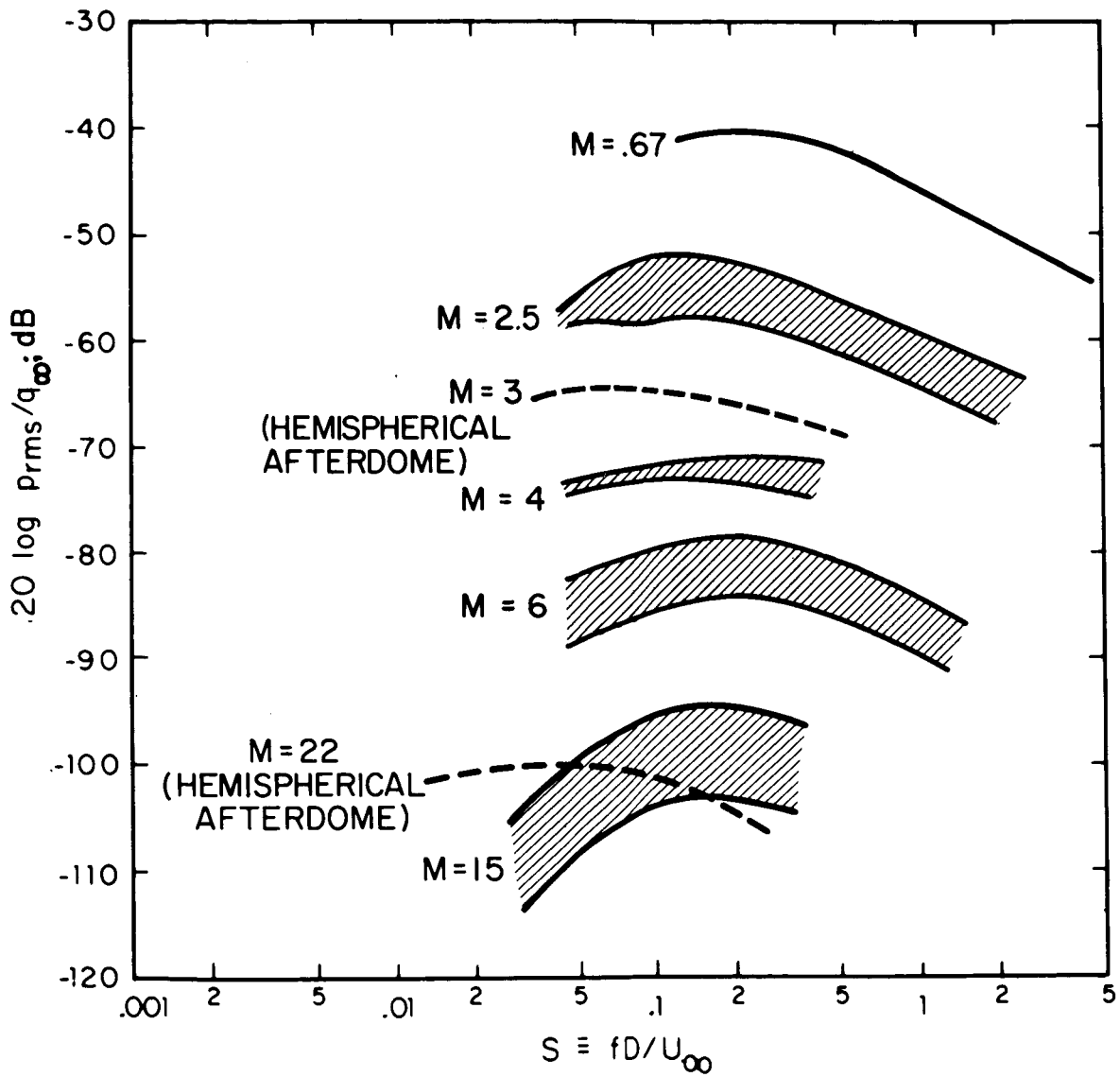
FIG. 38. NONDIMENSIONAL BASE-PRESSURE SPECTRA FOR VARIOUS
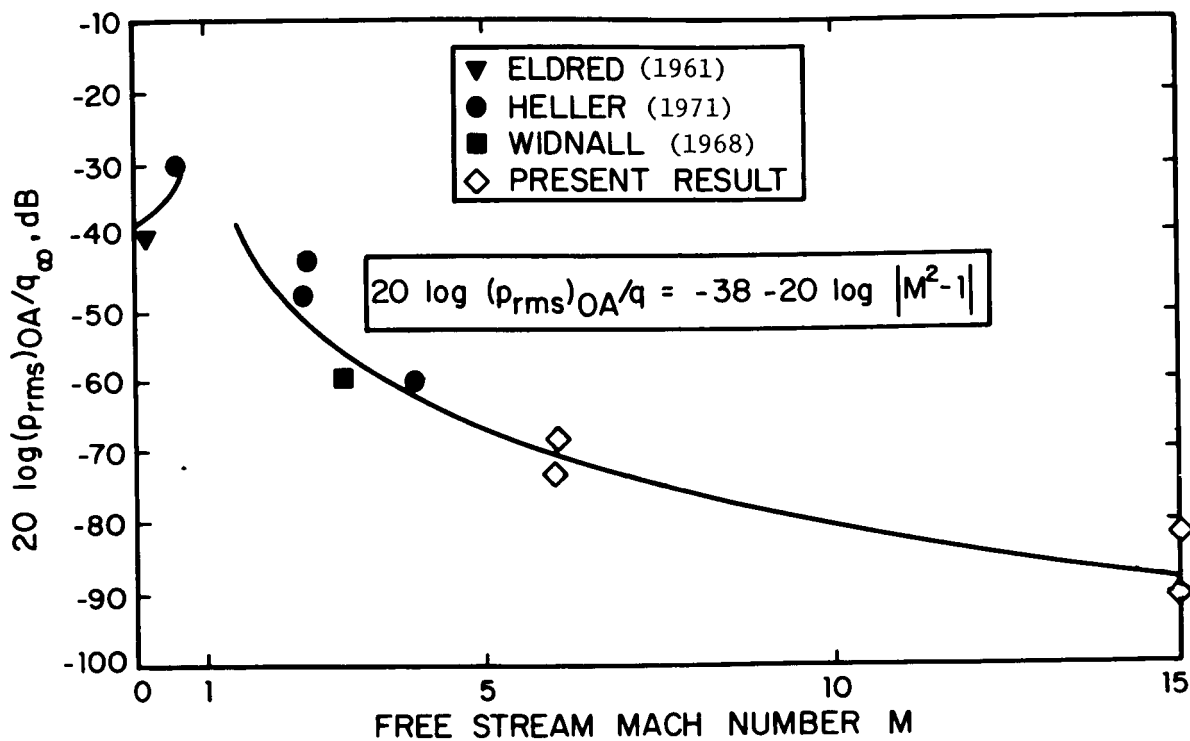FREE-STREAM MACH NUMBERS

FIG. 39. FREE-STREAM MACH-NUMBER DEPENDENCE OF NORMALIZED OVERALL BASE-PRESSURE LEVEL FOR SLENDER-CONE/FLAT-BASE CONFIGURATIONS
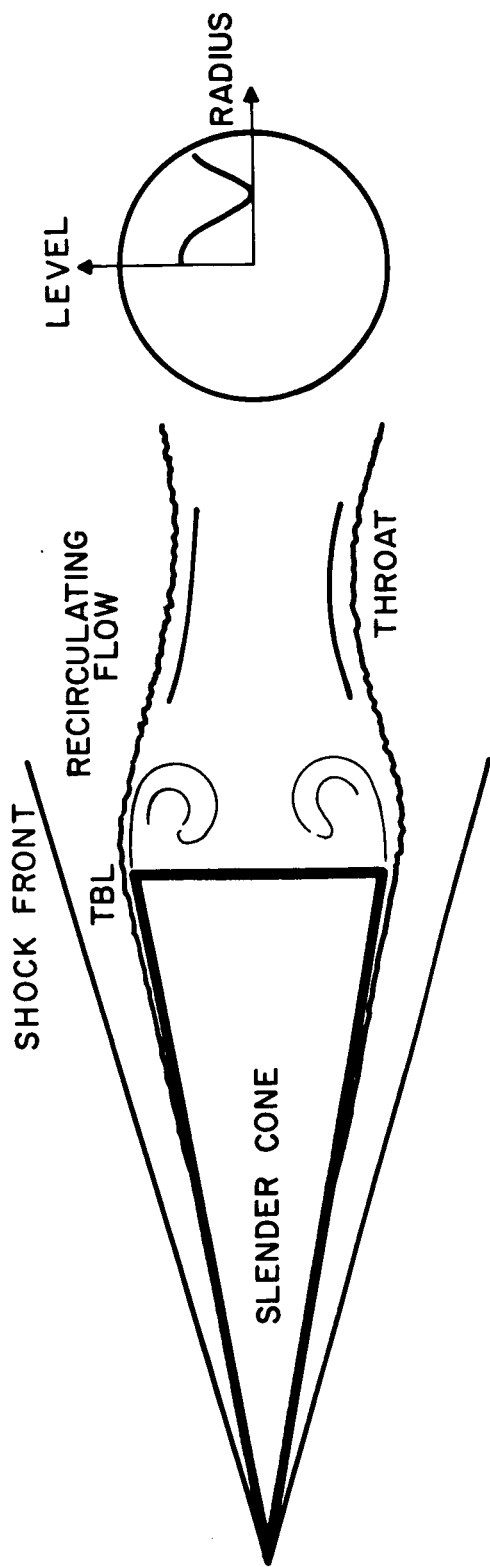
64

FIG. 40.   QUALITATIVE ILLUSTRATION OF OVERALL BASE-PRESSURE LEVEL WITH
RADIAL LOCATION ON BASE

65

INTERPRETATION OF TEST RESULTS

The VKI results for attached-flow surface pressure fluctuations and separated base-flow pressure fluctuations are compared to data obtained by Coe (1971), Martelucci (1972), and Widnall (1968). Preliminary analytical expressions are derived for the Mach-number dependence of the normalized overall fluctuating pressure. For reentry flight conditions, the Mach-number range of interest probably starts at Mach 20. In order to substantiate the proposed analytical expressions and to determine their validity range, wind tunnel tests at even higher Mach numbers should be conducted. However, such tests are not feasible since no facility has the required Reynolds-number capability.

Recently, data became available from an AVCO flight-test program on an 8° half-angle cone with a 1-m base diameter and a hemispherical afterdome at a free-stream Mach number of 22. The data were obtained through BBN furnished sensors; one was located at a mid-cone location; the other at the center of the base.

During the initial constant Mach-number reentry phase of this flight, the body experienced dynamic pressure changes of a factor of 25. Fluctuating-pressure levels under the attached turbulent boundary layer on the cone surface were found to scale very well with local dynamic pressure q_e (Fig. 41). Conversion into a 1/3-octave band spectrum provides the spectral peak; thus, the overall (nondimensional) level can be accurately determined.

Since there is no facility background noise in a free-flight test, and since the levels scale well with the dynamic pressure, we consider this data reliable. An empirical curve describing the overall pressure coefficient (p_{rms}/q) as function of Mach
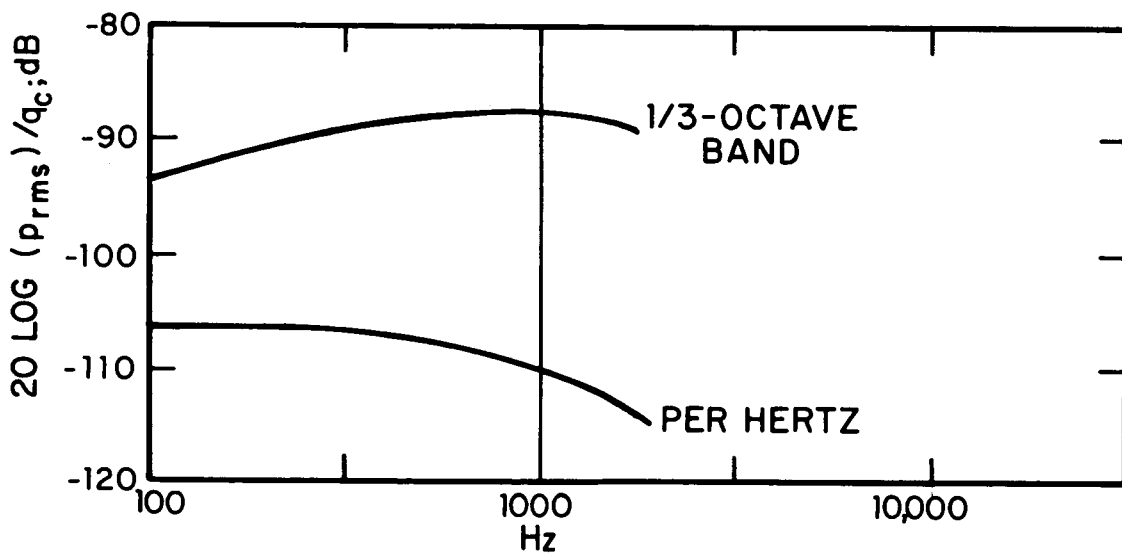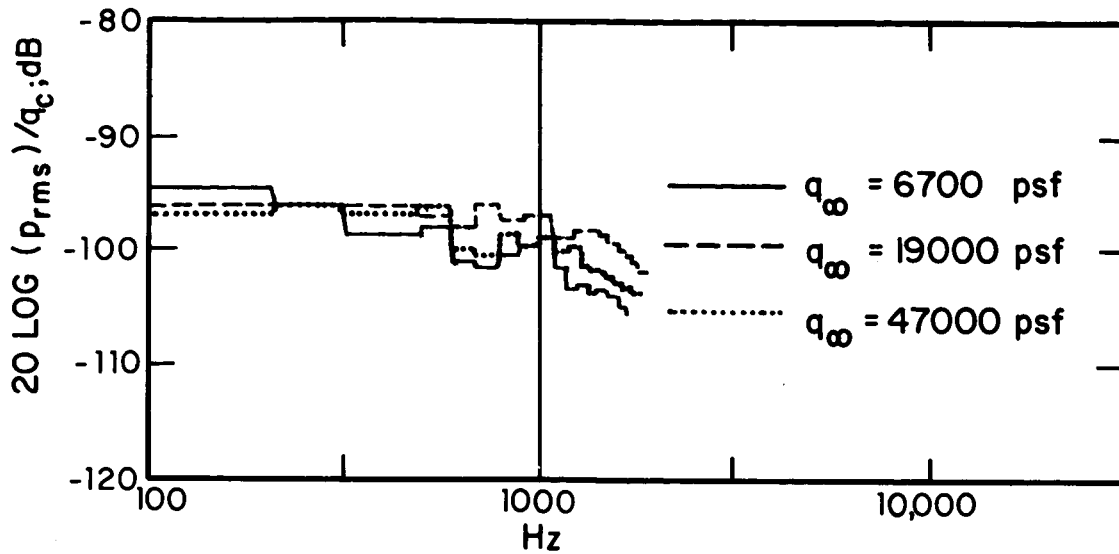
66

FIG. 41. FLUCTUATING-PRESSURE LEVEL SPECTRA UNDER ATTACHED
TURBULENT BOUNDARY LAYER ON CONICAL FLIGHT BODY
AT FREE-STREAM MACH NUMBER OF 22
(a) Normalized per-Hz spectrum
(b) Smoothed normalized per-Hz spectrum and
normalized 1/3-octave band spectrum

67

number, valid in the Mach-number range 0 < M < 12* (Fig. 42), can now be defined. This curve connecting the earlier MIT data, the data obtained in the present VKI effort, and the AVCO flight data with little scatter can be analytically expressed as

$$\frac{(P_{rms})_{overall}}{q_e} = \frac{0.006}{1 + (0.15M)^2 + (0.15M)^4} \quad .$$ (3)

We consider this expression is accurate within ±5 dB over the suggested Mach-number range. It should be noted that this plot uses the local Mach number. A vehicle reentering at a given free-stream Mach number will experience surface Mach numbers which are much lower than the free-stream Mach numbers, with correspondingly higher pressure coefficients and inherently higher loads.

The same flight test furnished base-pressure data that can validate the appropriate expression for the overall normalized base pressure as function of free-stream Mach number.

The raw data reduces to a normalized spectrum (Fig. 43), with a somewhat greater scatter than the "attached-flow data". In Fig. 44, a best-fit curve was drawn through the normalized spectrum and converted into a 1/3-octave band spectrum. Again, the overall pressure level can be determined accurately (see Fig. 45 also). By raising the previously proposed curve (Eq. 2) by 3 dB, a better data fit is obtained. The expression for the free-stream Mach-number dependence of the overall fluctuating base pressure now reads:

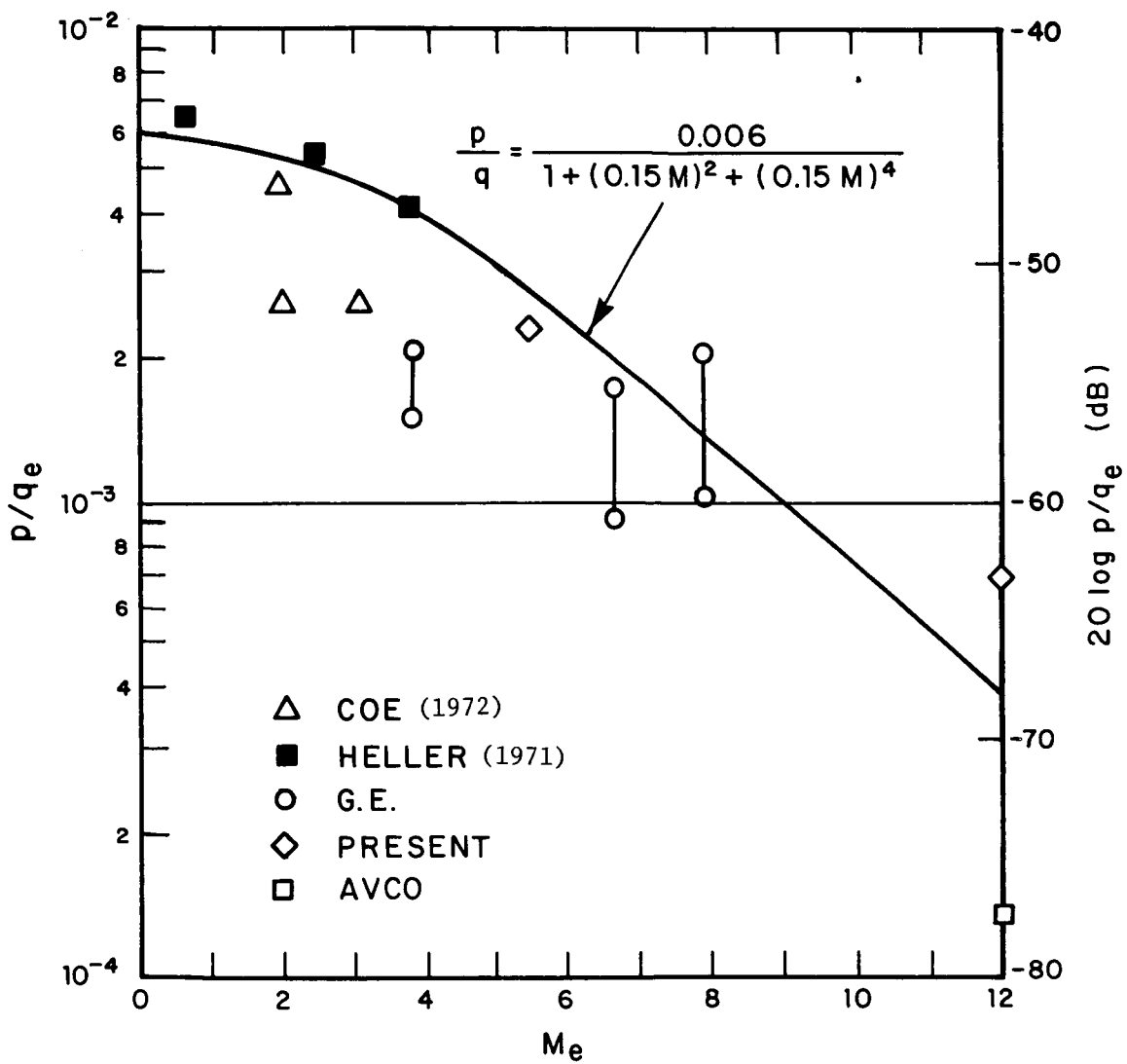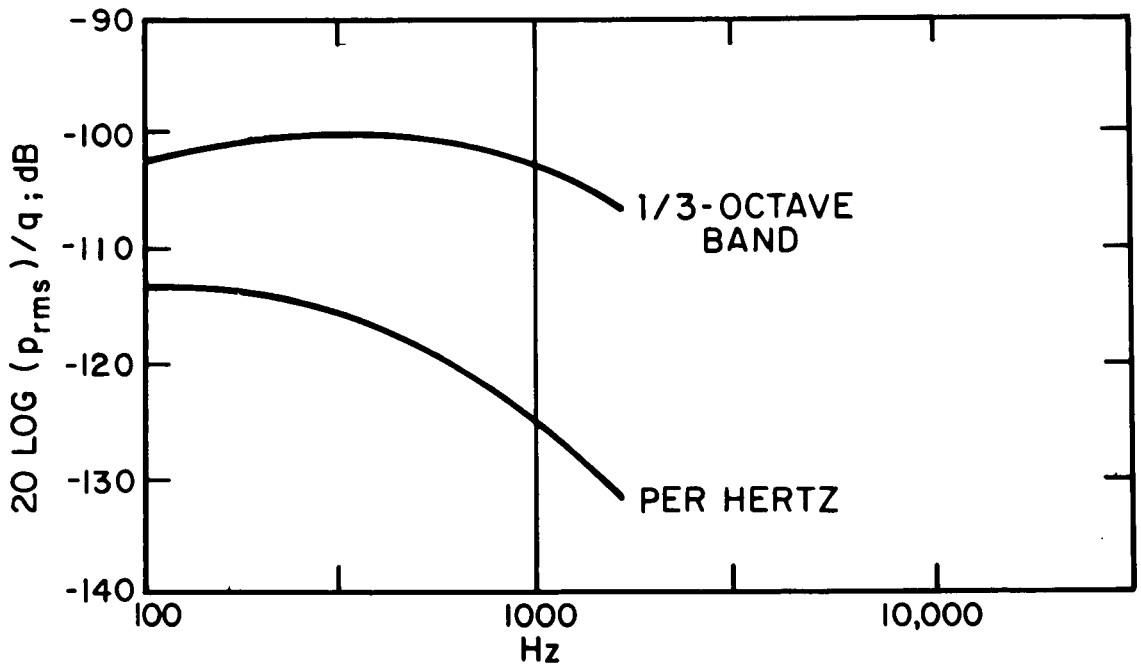*The edge Mach number on the cone for a free-stream Mach number of 22 is about 12.

FIG. 42. MACH-NUMBER DEPENDENCE OF OVERALL FLUCTUATING-
PRESSURE LEVEL UNDER ATTACHED TURBULENT
BOUNDARY LAYER

69
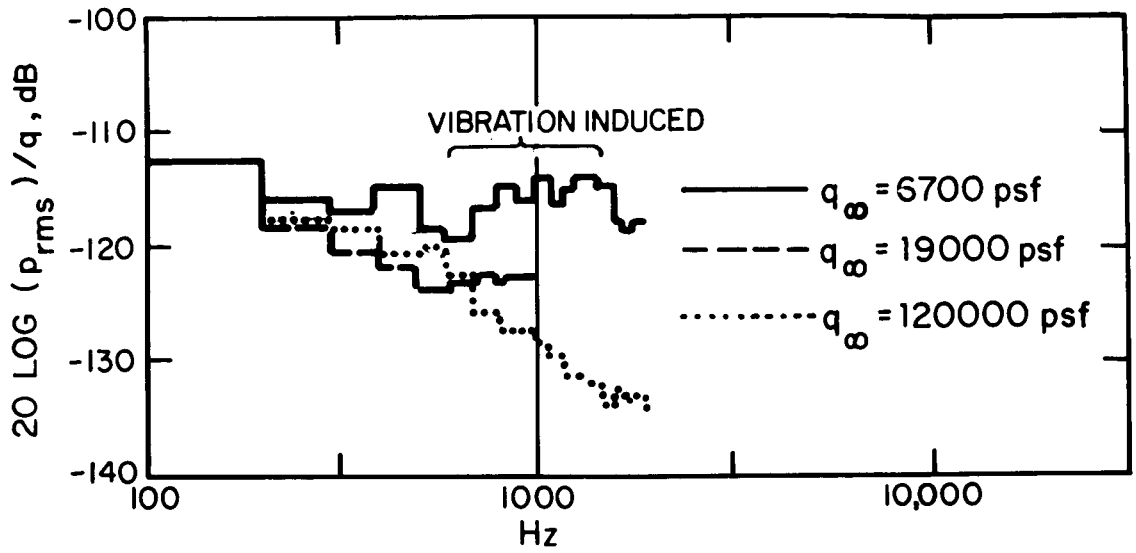
FIGS. 43 AND 44.   BASE-PRESSURE SPECTRA AT FREE-STREAM MACH
NUMBER OF 22

70

MACH NUMBER DEPENDENCE OF OVERALL
NORMALIZED FLUCTUATING BASE PRESSURE

$$20 \log (p_{rms})_{OA}/q_\infty = -35 -20 \log \left| M_\infty^2 -1 \right|$$

Legend:
- ▼ ELDRED (1961)
- ● HELLER (1971)
- ■ WIDNALL (1968)
- ◇ PRESENT RESULT
- ○ AVCO

FREE STREAM MACH NUMBER M_∞

$20 \log (p_{rms})_{OA}/q_\infty$; dB

FIG. 45. FREE-STREAM MACH-NUMBER DEPENDENCE OF NORMALIZED OVERALL BASE-PRESSURE
LEVEL FOR SLENDER-CONE/FLAT-BASE CONFIGURATIONS

$$20 \log (p_{rms})_{OA}/q = -35 - 20 \log |M^2-1| \quad . \qquad (4)$$
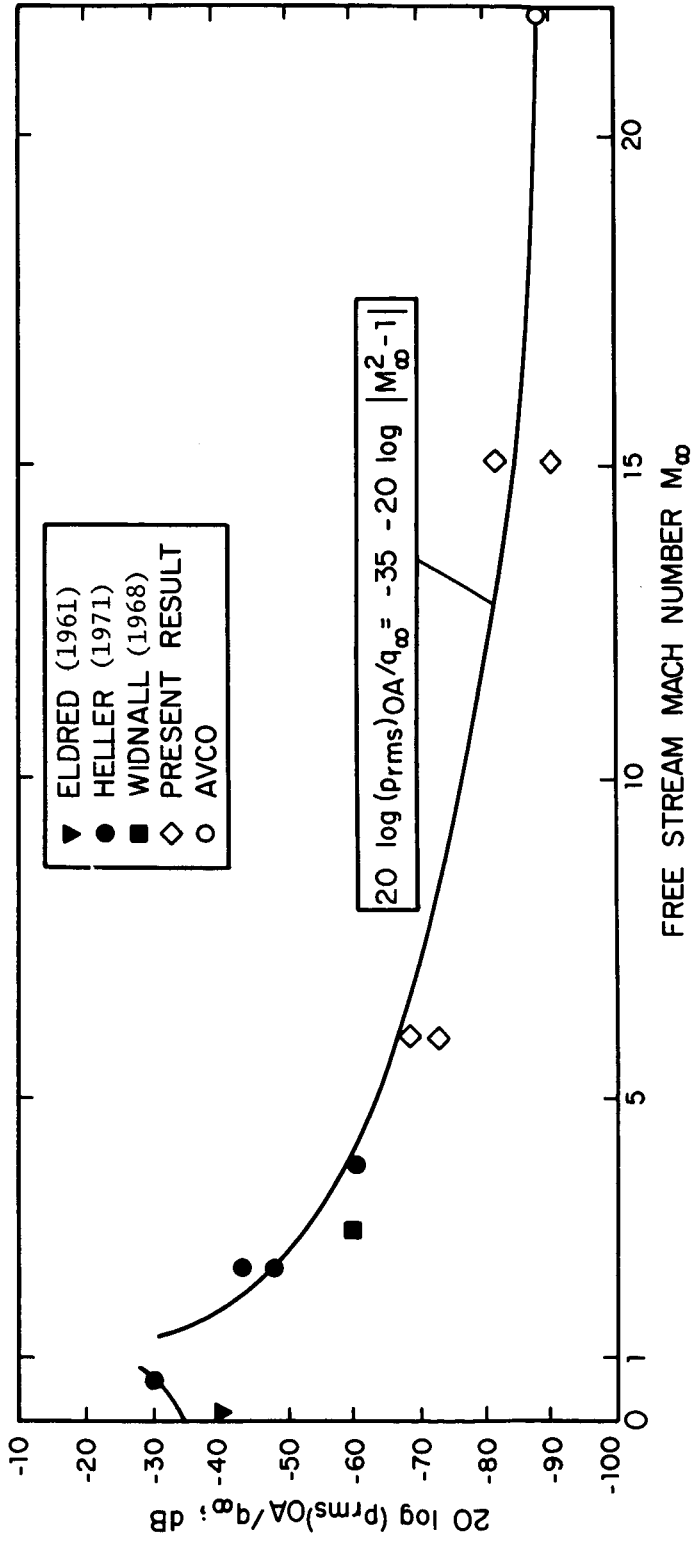
This equation seems to be valid in a free-stream Mach-number range from 0 to 22!

A comparison of the normalized base-pressure spectra of all available tests puts the Mach 22 spectrum peak at about $S_p \equiv f_p D/U_\infty = 0.04$; in previous tests, it was about 0.15 (see Fig. 38). However, the free-flight body has a hemispherical afterdome, while the wind tunnel models have a flat base. We have available some base-pressure data obtained by Widnall (1968) on an 8° half-angle cone/hemispherical base model at Mach 3. Presented in Fig. 38, this spectrum seems to indicate a peak near 0.06. However, not enough data for cone/hemispherical afterdome configurations are available to define this trend.

The FPL spectrum under the attached boundary layer for Mach 22 flow is available and probably represents an accurate test result. However, local boundary-layer dimensions were not obtained to nondimensionalize this spectrum and put it in the context of other research results.

CONCLUSIONS

It has been shown that simple expressions describe the variation with Mach number of the overall pressure coefficient $C_p \equiv (p_{rms}/q)$ for attached turbulent flow and for separated base flow. To substantiate these expressions, results from six different research efforts, including one flight test, were utilized.

More work is necessary to obtain a nondimensional turbulent boundary-layer spectrum that is valid over a Mach-number range up to hypersonic speeds. Other areas of uncertainties are the following: the overall pressure coefficient for base pressures at subsonic, transonic, and low supersonic Mach numbers; and the relative levels, shape, and spectral peak of the nondimensional base-pressure spectrum for various base geometries and locations in the base regime of slender cones.

REFERENCES

Chandiramani, K., *et al* (1966). "Structural Response to Inflight Acoustic and Aerodynamic Environments," BBN Report No. 1554 (Confidential).

Coe, C.F. and Chyu, W.J. (1972). "Pressure Fluctuation Inputs and Response of Panels Underlying Attached and Separated Supersonic Turbulent Boundary Layers," presented at the AGARD Symposium on Acoustic Fatigue, Toulouse, France.

Coe, C.F., Dods, Jr., J.B., Robinson, R.C., and Mayes, W.H. (1971). "Preliminary Measurements and Flow Visualization Studies of Pressure Fluctuations on Space Shuttle Configurations," NASA Space Shuttle Technology Conference Vol. III — Dynamics and Aeroelasticity, NASA TM X-2274.

Eldred, K. McK. (1961). "Base Pressure Fluctuations," *J. Acoust. Soc. Am.* **33**(1):59.

Heller, H.H. and Holmes, D.G. (1971). "Unsteady Aerodynamic Loads During Reentry of the Straight-Wing Orbiter Configuration," NASA CR 111960.

Martellucci, A., Chaump, L., and Rogers, D. (1972). "Experimental Determination of the Aeroacoustic Environment About a Slender Cone," AIAA Paper No. 72-706.

Widnall, S.E. (1968). "Fluctuating Pressure Measurements on a Slender Cone Model in Mach 3 Flow," BBN Tech Memo No. 1, Job 151194.

APPENDIX A

1. The VKI Longshot Free-Piston Tunnel

2. The VKI Hypersonic Tunnel H-3

Description

The VKI Longshot free-piston tunnel is an intermittent facility operating with nitrogen, designed for the attainment of very high Reynolds-number hypersonic flows. It has a conical nozzle of 36 cm (14 in.) exit diameter and an open-jet test section. Longshot differs from a conventional gun tunnel in that a heavy piston is used to compress the test gas, which is trapped in a reservoir at the end of the barrel at peak pressure and temperature by the closing of a system of check valves as the piston rebounds. Instrumentation includes 16 channels of thin-film heat-transfer gauges, 8 channels of piezo-electric and diaphragm-type pressure gauges, a laser integrating schlieren system for flow field density measurements, and a conventional schlieren for flow visualization. Static and dynamic stability measurements are made by taking high-speed motion pictures of free-flight models.

Performance

Mach number: 15 – 20. Reynolds number/ft: 3×10^6 to 10×10^6. Supply pressure: 60,000 psi (max). Supply temperature: 2600° K (max). Running time: 10 – 40 msec. Shots per day: 2.

Note: For a complete description of the facility capabilities, see article in *AIAA Journal* (1970), 8(6):1020.

Type of Research

Laminar and turbulent heat transfer. Boundary-layer transition. Static and dynamic stability. Flow field around bodies.

Theoretical and experimental studies of dense gas effects in the piston cycle and nozzle expansion processes.

Description

The VKI hypersonic tunnel H-3 is an intermittent facility of the blow-down type with an axisymmetric nozzle giving a uniform free jet 12 cm in diameter (5 in.), followed by an adjustable diffuser. Air is supplied from storage tanks [60 m³ (2100 ft³) at 40 bars (570 psi) and 14 m³ (500 ft³) at 300 bars (4300 psi)] through a pebble-bed heater. A supersonic ejector is used to provide the necessary suction downstream of the diffuser. The test section contains a precision three-degree-of-freedom traversing mechanism for model and/or probe support, as well as variable incidence mechanism (-5 to +5 degrees). The tunnel is equipped with shadow and double-pass schlieren systems. Instrumentation includes differential transducers and scani-valves for pressure measurements, a three-component strain gauge balance, and equipment for heat-transfer measurements.

Performance

The range of stagnation pressure is from 7 to 35 bars abs (100 to 500 psi). The maximum stagnation temperature is 450° C (840° F). The minimum ejector suction without secondary flow is 0.01 bar abs (0.14 psia). The Mach number of the uniform free jet is M=6.0. The unit Reynolds number can be varied between 2 and 10×10^6/m. Running times up to 5 min are available.

Type of Research

Boundary-layer studies, separated flows, and shock-wave boundary-layer interactions.